

This is an Open Access document downloaded from ORCA, Cardiff University's institutional repository: <https://orca.cardiff.ac.uk/id/eprint/94065/>

This is the author's version of a work that was submitted to / accepted for publication.

Citation for final published version:

Gurenko, Andrey A., Kamenetsky, Vadim S. and Kerr, Andrew C. 2016. Oxygen isotopes and volatile contents of the Gorgona komatiites, Colombia: A confirmation of the deep mantle origin of H₂O. *Earth and Planetary Science Letters* 454 , pp. 154-165. 10.1016/j.epsl.2016.08.035

Publishers page: <http://dx.doi.org/10.1016/j.epsl.2016.08.035>

Please note:

Changes made as a result of publishing processes such as copy-editing, formatting and page numbers may not be reflected in this version. For the definitive version of this publication, please refer to the published source. You are advised to consult the publisher's version if you wish to cite this paper.

This version is being made available in accordance with publisher policies. See <http://orca.cf.ac.uk/policies.html> for usage policies. Copyright and moral rights for publications made available in ORCA are retained by the copyright holders.



1
2
3
4
5
6
7
8
9
10
11
12
13
14
15
16
17
18
19
20
21
22
23
24
25
26

**Oxygen isotopes and volatile contents of the Gorgona komatiites, Colombia: a confirmation
of the deep mantle origin of H₂O**

Andrey A. Gurenko^{1*}, Vadim S. Kamenetsky², Andrew C. Kerr³

¹ *Centre de Recherches Pétrographiques et Géochimiques, UMR 7358, Université de Lorraine,
54501 Vandoeuvre-lès-Nancy, France*

² *School of Physical Sciences, University of Tasmania, Private Bag 79, Hobart, TAS 7001,
Australia*

³ *School of Earth and Ocean Sciences, Cardiff University, Park Place, Cardiff, UK, CF10 3AT*

Revised manuscript

submitted to *Earth and Planetary Science Letters*

10 August, 2016

Components: abstract (333 words; 2,114 characters with spaces),
main text (8,258 words; 53,382 characters with spaces),
6 figures, 0 tables,
the list of references includes 102 citations.

* **Corresponding author and present address:** Andrey A. Gurenko, Centre de Recherches Pétrographiques et
Géochimiques, 15, rue Notre-Dame des Pauvres, BP 20, 54501 Vandoeuvre-lès-Nancy, France. Phone: +33 (0)3 83
59 48 75, Fax: +33 (0)3 83 51 17 98, E-mail: agurenko@crpg.cnrs-nancy.fr

27 **Abstract**

28 We report O isotopes in olivine grains (F_{O89-93}) and volatile contents (CO₂, H₂O, F, S, Cl) in
29 olivine-hosted melt inclusions from one Gorgona picrite and five komatiites with the aim of
30 constraining the origin of H₂O in these magmas. These samples have previously been analysed
31 for major and trace elements and volatile concentrations (H₂O, S, Cl) and B isotopes in melt
32 inclusions. A distinctive feature of the included melts is relatively high contents of volatile
33 components and boron, which show positive anomalies in, otherwise depleted, primitive mantle
34 normalised trace and rare earth element patterns and range in $\delta^{11}\text{B}$ from -11.5 to 15.6% . In this
35 study, the olivines were systematically analysed for O isotopes (1) in the centre of grains, (2)
36 near the grain boundaries and, (3) as close as possible to the studied melt inclusions. The
37 majority of olivines ($\sim 66\%$) are “mantle”-like, $4.8\% \leq \delta^{18}\text{O} \leq 5.5\%$, with a subordinate but still
38 significant number ($\sim 33\%$) above, and only 2 grains below, this range. There is no systematic
39 difference between the central and marginal parts of the grains. Higher than “mantle” $\delta^{18}\text{O}_{\text{O1}}$
40 values are ascribed to low- T (< 300 °C) serpentinisation along inner fractures and grain
41 boundaries of olivine phenocrysts. The measured concentrations of volatile components in the
42 melt inclusions corrected for the effects of post-entrapment crystallisation and H₂O-CO₂
43 exsolution in inclusion shrinkage bubbles are: 286–1748 $\mu\text{g/g}$ CO₂, 0.2–0.86 wt.% H₂O, 48–82
44 $\mu\text{g/g}$ F, 398–699 $\mu\text{g/g}$ S and 132–198 $\mu\text{g/g}$ Cl. They correspond to a pressure of 86 ± 44 MPa or
45 ~ 2.5 -km crustal depth of olivine crystallisation. The correlations of S and, to a lesser extent, of
46 H₂O, with highly incompatible lithophile elements and the correlation of F with Cl, but no
47 relationships of H₂O with Cl, rule out shallow depth magma degassing and/or crustal
48 contamination. Our new $\delta^{18}\text{O}$ olivine and volatile component data combined with the existing,
49 highly variable $\delta^{11}\text{B}$ values for melt inclusions also support the deep mantle origin of H₂O (and
50 probably other volatiles) in the Gorgona mafic and ultramafic magmas.

51

52

53 **Keywords**

54 Gorgona Island, Komatiites, Olivine, Oxygen isotopes, Volatile components, Ion microprobe

55

56

57 **1. Introduction**

58 Komatiites are olivine spinifex-textured, ultramafic, mantle-derived rocks formed by high
59 degrees of partial melting and typically having high magnesium (>18 wt.% MgO), with low
60 silicon (40–45 wt.% SiO₂), titanium (<1 wt.% TiO₂) and incompatible trace element
61 concentrations (e.g., [Arndt and Nisbet, 1982](#); [Kerr and Arndt, 2001](#) and references therein).
62 Komatiites were first recognized in the late 1960s in the Barberton greenstone belt, South Africa,
63 and were named from their type locality along the Komati River ([Viljoen and Viljoen, 1969a,b](#)).
64 There has long been a considerable debate as to whether komatiites are derived from dry and hot
65 mantle, and are the products of partial melting of ascending super-hot Archaean plumes (e.g.,
66 [Bickle et al., 1977](#); [Campbell et al., 1989](#); [McDonough and Ireland, 1993](#); [Arndt et al., 1997](#),
67 [1998](#); [Herzberg et al., 1995, 2007](#); [Berry et al., 2008](#) among others) or are formed by hydrous
68 melting of the mantle at much lower temperatures during subduction (e.g., [Allègre, 1982](#);
69 [Parman et al., 1997](#); [Grove and Parman, 2004](#); [Parman and Grove, 2005](#)). Because most
70 komatiites have undergone significant sub-solidus alteration, primary volatile abundances of the
71 magmas from which they crystallised, remain controversial.

72 In this context, the Late Cretaceous (~90 Ma) ultramafic and mafic lavas of the Gorgona
73 Island, Colombia, first identified as komatiites by [Gansser et al. \(1979\)](#) and then studied in more
74 detail by e.g., [Echeverría \(1980\)](#), [Dietrich et al. \(1981\)](#), [Aitken and Echeverría \(1984\)](#),
75 [Echeverría and Aitken \(1986\)](#), [Kyser et al. \(1987\)](#), [Kerr et al. \(1996\)](#), [Arndt et al \(1997\)](#), [Kerr](#)
76 [\(2005\)](#), [Révillon et al. \(2000, 2002\)](#), [Serrano et al. \(2011\)](#), among others, represent suitable
77 candidates for the study of volatile components because they are generally much fresher
78 compared to most of their Archaean counterparts. In addition, the komatiites from Gorgona
79 remain the only known non-Archaean komatiites and, therefore, studying them in detail may
80 have important implications for our understanding the effects of water on mantle potential
81 temperatures.

82 Although, overall, olivine-hosted melt inclusions in Gorgona komatiites are depleted in
83 incompatible trace elements, they are distinctive in that they possess relatively high
84 concentrations of volatile components and boron (Kamenetsky et al., 2010). These high
85 concentrations result in positive anomalies (10 to 50 fold enrichment) on primitive mantle
86 normalised trace and rare earth element diagrams and a wide range of $\delta^{11}\text{B}$ values from -11.5 to
87 $+15.6\%$. Based on these data, Gurenko and Kamenetsky (2011) concluded that the inclusions
88 with “mantle”-like $\delta^{11}\text{B}$ (around -10%), also enriched in H_2O and Cl , represent the unmodified
89 composition of their parental magmas. Moreover, they demonstrated that although a range of
90 contaminants (seawater, NaCl saline brines, altered oceanic crust, serpentinised peridotite or
91 marine sediments) could potentially affect the composition of these magmas, the observed
92 volatile enrichment could be better explained by possible input of less than 3 wt.% of a H_2O - and
93 ^{11}B -enriched fluid into the source of the Gorgona komatiites.

94 The present work is follow-up study (from the work of Kamenetsky et al., 2010);
95 Gurenko and Kamenetsky, 2011) on olivines from Gorgona komatiites and their included melts
96 and primarily focuses on their detailed oxygen isotopic composition, determined by SIMS (=
97 Secondary Ion Mass Spectrometry). The main purpose of the present study is therefore to further
98 constrain the origin of volatile components, and especially H_2O in the Gorgona parental magmas.
99 Furthermore, in order to evaluate the pressure (or depth) of olivine crystallization (with the aim
100 of discriminating between upper and lower crust levels, which presumably have different O-
101 isotope signatures), and to place additional constraints on the behaviour of volatile components
102 during magma origin and consequent crystallization, we re-analysed the same olivine-hosted
103 melt inclusions remaining after the Kamenetsky et al. (2010) and Gurenko and Kamenetsky
104 (2011) SIMS and laser ablation ICP-MS measurements. These previously studied melt
105 inclusions, together with several newly exposed inclusions were analysed for CO_2 , H_2O , F , S and
106 Cl (note that neither CO_2 nor F concentrations were previously reported). Based on the existing

107 and our new volatile component and O-isotope data, this study will help to determine if the
108 ascending high-Mg melts, currently preserved as inclusions in olivine, have suffered
109 contamination by either crustal rocks at shallow depth (Arndt et al., 1997), or by seawater or
110 seawater-derived components (Shimizu et al., 2009). If such contamination has occurred, one
111 would expect a deviation of $\delta^{18}\text{O}$ measured in the studied Gorgona olivines from that of the
112 mantle (4.8–5.8‰; Matthey et al., 1994; Eiler, 2001) to more ^{18}O -enriched values. In this context,
113 our new oxygen isotope data on olivines, when coupled with the available volatile contents and
114 boron isotope data on melt inclusions will be key to unravelling the origin of wet high-Mg
115 magmas, now preserved as komatiites and picrites on the island of Gorgona.

116

117 **2. Geological setting and samples**

118 Gorgona is located ~40 km off the Pacific coast of Colombia (**Fig. 1**). The geology of this
119 small island (approximately 8.3 km long and 2.5 km wide), was first studied by Gansser (1950),
120 who noted the occurrence of “olivine rocks” containing skeletal olivine phenocrysts, which later
121 were recognised as “komatiites” by Gansser et al (1979) and Echeverría (1980). Echeverría
122 (1980) also reported picrites from the south part of the island that had no skeletal olivine crystals.
123 An undeformed peridotite-gabbro complex is located in the central part of the island and
124 surrounded by a sequence of tilted and faulted blocks of mafic and ultramafic rocks and tuff
125 breccias (Dietrich et al., 1981; Aitken and Echeverría, 1984). The first petrographic and
126 geochemical work on these rocks was reported by Dietrich et al. (1981) and Echeverría (1980)
127 and demonstrated that the olivine spinifex (komatiite) lavas contain 13 to 24 wt.% MgO. Aitken
128 and Echeverría (1984) proposed that the parental magma of the komatiites contained ~20 wt.%
129 MgO. Kyser et al. (1987) reported the first stable isotope (δD and $\delta^{18}\text{O}$) data on Gorgona
130 komatiites.

131 Our present work is based on the same 50 olivine fragments studied by [Kamenetsky et al.](#)
132 [\(2010\)](#) and [Gurenko and Kamenetsky \(2011\)](#). These fragments contain small portions of melt
133 entrapped along zones of skeletal growth of the former euhedral to subhedral olivine
134 phenocrysts, as well as 21 additional, randomly selected olivine phenocrysts from a picrite
135 sample GOR94-32. The komatiitic samples were collected from fresh coastal exposures on the
136 north east side of the island (**Fig. 1**; for more detail, see [Kamenetsky et al., 2010](#)).

137 Sample GOR94-32 was collected from a picrite lava block, whose whole rock
138 geochemistry was reported by [Arndt et al. \(1997\)](#). As first noted by [Echeverría and Aitken](#)
139 [\(1986\)](#) and studied subsequently by [Kerr et al. \(1996\)](#), [Révillon et al. \(2000\)](#) and [Kerr \(2005\)](#), the
140 fragmental picritic rocks (with angular-to-rounded blocks ranging in size from a few centimetres
141 to > 1 m) and picritic tuffs are exposed in the southern part of the island and are intruded by a
142 suite of comagmatic dykes (**Fig. 1**). As noted by [Kerr \(2005\)](#), the picrite blocks comprise ~25
143 vol.% euhedral, non-skeletal olivine phenocrysts (0.5–1.0 mm), set in a groundmass of very fine-
144 grained Cr-spinel microphenocrysts and acicular crystals of clinopyroxene and plagioclase.

145

146 **3. Analytical methods**

147 Oxygen isotopic composition of olivine grains was systematically analysed by ion
148 microprobe. Several previously studied and newly exposed olivine hosted melt inclusions were
149 also analysed for CO₂, H₂O, F, S and Cl concentrations by SIMS. In order to check that no host
150 olivine was ablated by the ion beam, the spot position was carefully examined with a
151 petrographical microscope after analysis. As an additional check, aluminium (since it is
152 incompatible in olivine but present in the melt inclusions in concentrations >15 wt.% Al₂O₃) was
153 also included in the analytical sequence along with the volatile components in order to monitor
154 and correct for any ablation of olivine (for more detail, see *Supporting online material*).
155 Following these analyses, olivine composition was re-analysed by electron microprobe (hereafter

156 EPMA = Electron Probe Microanalysis) as close as possible (10–30 μm) to the spots left by
157 SIMS. Most of the studied olivines were analysed for major elements by [Kamenetsky et al.](#)
158 [\(2010\)](#). However, here we report and discuss only the newly acquired olivine major element
159 data, except for four olivine grains that were lost during remounting from an epoxy mount into
160 indium metal. For these olivines, we use major element compositions published in [Kamenetsky](#)
161 [et al. \(2010\)](#).

162

163 **4. Results**

164 *4.1. Elemental and oxygen isotope variability of olivines*

165 The olivines were systematically analysed for oxygen isotopes: a) in the centre of grain,
166 b) near the grain boundaries and c) as close as possible to the previously studied and newly
167 exposed melt inclusions. As noted by [Kamenetsky et al. \(2010\)](#), olivine phenocrysts from the
168 studied komatiite samples are serpentinised along inner fractures and grain margins.
169 Consequently only smaller fragments of former olivine phenocrysts remained intact for
170 geochemical analysis and the melt inclusion study. For this reason, no direct link exists between
171 internal and external parts of the analysed grains and the true cores and rims of the former
172 olivine crystals.

173 The analyses of oxygen isotopes were replicated 2 to 28 times (except for 2 of 71 olivine
174 grains that were analysed only in one spot) during three separate analytical sessions (for
175 reproducibility results, see **Fig. S1.1** of *Supporting online material*). In total, 138 oxygen isotope
176 analyses of olivine, each based on an average of up to 14 spot analyses (in total 824 individual
177 $^{18}\text{O}/^{16}\text{O}$ determinations) were completed during the present study.

178 The olivines from the Gorgona picrite sample (GOR94-32) have a wider range of
179 forsterite contents that extend to higher values ($\text{Fo}_{88.3-93.2}$), as compared to those from the
180 komatiite samples ($\text{Fo}_{88.3-91.5}$), and contain 0.29–0.38 wt.% CaO, 0.34–0.46 wt.% NiO,

181 0.09–0.19 wt.% Al₂O₃ and 0.07–0.17 wt.% Cr₂O₃). However, the olivines from this picrite have
182 systematically lower NiO concentrations than the komatiite olivines at equivalent Fo contents,
183 resulting in two distinct trends of olivine crystallisation (**Fig. 2a, b**). These trends are in
184 agreement with the observation of [Kerr et al. \(1996\)](#), who noted that Gorgona picrites usually
185 have lower Fe₂O₃, Ni and Zr and somewhat higher Sc and Y concentrations (at a given MgO)
186 than the komatiites. We think that the observed narrow Fo-ranges within individual samples
187 ($\Delta\text{Fo} = \text{Fo}_{\text{max}} - \text{Fo}_{\text{min}}$ for a given sample is between 0.6 and 3.2 mol.% in komatiites and 4.9
188 mol.% in picrite; **Fig. 2a**), similar concentrations of NiO (0.36–0.50 wt.%, except for one grain
189 with 0.32 wt.%; **Fig. 2b**), CaO (0.3–0.36 wt.%, except for one grain with 0.4 wt.%), Al₂O₃
190 (0.07–0.14 wt.%) and Cr₂O₃ (0.07–0.15 wt.%) (**Table S2.1 – Supporting online material**), and
191 almost complete overlap of the compositions of the internal and external parts of the studied
192 olivine fragments imply almost no elemental intra-crystal zoning.

193 The $\delta^{18}\text{O}_{\text{Ol}}$ span a range of values between 4.7 and 6.0‰ (**Fig. 2c, d**). Because most
194 individual grains were multiply analysed in the centre of the grain and near the grain boundaries,
195 the average external precision of $\delta^{18}\text{O}_{\text{Ol}}$ determinations in the internal and external grain zones is
196 $\pm 0.2\text{‰}$, 2 SE (broad range is 0.07–0.47‰). The majority of $\delta^{18}\text{O}_{\text{Ol}}$ values (~66% i.e., 91 of 138)
197 are mantle-like, with $\delta^{18}\text{O}_{\text{Ol}}$ ranging from 4.8 to 5.4‰. A significant number of $\delta^{18}\text{O}_{\text{Ol}}$
198 determinations (~33%, i.e., 45 of 138) exceed the “mantle” range towards higher values, and
199 only two of 138 are below 4.8‰. The probability density distribution curves calculated using
200 *Isoplot 3.70* ([Ludwig, 2008](#)) reveal a common maximum of $\delta^{18}\text{O}_{\text{Ol}}$ at ~5.3‰ for most of the
201 studied olivine “cores” and “rims” (**Fig. 2e**), but the “rims” exhibit also an additional,
202 subordinate peak at ~5.6‰. The absence of systematic differences (or zoning) in both Fo and
203 $\delta^{18}\text{O}_{\text{Ol}}$ values between internal and external parts of the grains can be interpreted as evidence for
204 only minor interaction of the crystallised olivines with a second primitive or evolved magma, or
205 interaction of the olivine parental magma with surrounding crustal rocks.

206 Prior to this study only a limited amount of oxygen isotope data was available for
207 Gorgona mafic rocks: [Kyser et al. \(1987\)](#) reported (from two basalts and one picrite) a range of
208 $\delta^{18}\text{O}$ from 6.0 to 6.3‰ for olivine and 7‰ for one clinopyroxene. The results of this study were
209 interpreted as supporting a mantle origin of the Gorgona komatiites, suggesting that the mantle
210 source of these rocks may have been more fertile, compared to that of Archaean komatiites.
211 Moreover, the δD and $\delta^{18}\text{O}$ values obtained for chrysolite from Gorgona komatiitic samples by
212 [Kyser et al. \(1987\)](#) were interpreted to be consistent with serpentinisation by meteoric water
213 rather than from seawater. A subsequent study by [Révillon et al. \(2002\)](#) reported a $\delta^{18}\text{O}$ range
214 from 5.25 to 5.73‰ for clinopyroxene separates from the Gorgona picrites and komatiites.
215 Accordingly, using the oxygen isotope fractionation factor between olivine and clinopyroxene
216 ($\Delta^{18}\text{O}_{\text{Cpx-Ol}} = 0.33\text{--}0.37$; [Chiba et al., 1989](#)), the $\delta^{18}\text{O}_{\text{Ol}}$ equivalent calculated for 1300–1400°C
217 using the above clinopyroxene O-isotope data is in the range of 4.9–5.4‰, i.e., values that are
218 similar to the O-isotope range obtained in the present study.

219

220 *4.2. Volatile concentrations*

221 As previously shown by [Kamenetsky et al. \(2010\)](#) and [Gurenko and Kamenetsky \(2011\)](#),
222 melt inclusions from the studied Gorgona olivines are characterised by pronounced enrichment
223 of volatile components (0.2–1.0 wt.% H_2O , 520–770 $\mu\text{g/g}$ S, 220–310 $\mu\text{g/g}$ Cl) and boron
224 (0.61–2.02 $\mu\text{g/g}$ B) which show positive anomalies in, otherwise depleted, primitive mantle
225 normalised trace element and REE patterns. In order to constrain a minimum pressure (or depth)
226 of olivine crystallisation (with the aim of discrimination between upper and lower crustal rocks
227 that have different O-isotope composition; e.g., [Gregory and Taylor, 1981](#)), and to place
228 additional constraints on the behaviour of volatile components during magma origin and
229 consequent crystallization, we re-analysed 6 melt inclusions remaining after SIMS and laser
230 ablation ICP-MS measurements, whose compositions are reported in [Kamenetsky et al. \(2010\)](#)

231 and [Gurenko and Kamenetsky \(2011\)](#), and analysed 9 additional melt inclusions for CO₂, H₂O,
232 F, S and Cl by SIMS. More detailed information about the selection and preparation of melt
233 inclusions prior to analysis, and their laboratory heating and quenching conditions is given in
234 [Kamenetsky et al. \(2010\)](#). No melt inclusions in olivine from the picrite sample GOR94-32 were
235 analysed during the present study.

236 Prior to interpreting the existing volatile data it is important to assess whether the original
237 concentrations of water dissolved in the included melts are compromised by possible diffusive
238 gain or loss of H₂O through olivine host. Such diffusion of H₂O was first noted by [Sobolev and](#)
239 [Danyushevsky \(1994\)](#) and then experimentally investigated by [Portnyagin et al. \(2008\)](#) and other
240 more recent studies. The problem of possible rapid exchange of water between melt inclusions in
241 olivine and a host magma in relation to the studied Gorgona melt inclusions were briefly
242 discussed in [Kamenetsky et al. \(2010\)](#), who have concluded that “...the enrichment of the
243 studied melt inclusions in the volatile elements is magmatic in origin” (page 1005). Moreover, if
244 H₂O was acquired by the inclusions due to H⁺-diffusion inside olivine hosts, this would imply
245 the existence of a H₂O-rich ambient magma, from which the olivines with “normal mantle” $\delta^{18}\text{O}$
246 signature have crystallized. The existence of such a H₂O-rich magma would additionally support
247 our previous conclusion about wet origin of the Gorgona komatiites. We thus maintain that the
248 only process that could potentially bias water concentrations is H₂O-loss that could also happen
249 during laboratory heating of the inclusions. However, several lines of evidence argue against
250 extensive loss of H₂O during olivine crystallisation at depth or upon eruption:

251

- 252 1. The first and compelling evidence arguing against possible diffusive gain or loss of H₂O is
253 existence of multiple significant correlations between volatile components, especially H₂O,
254 and major (SiO₂ in the case of H₂O) and multiple incompatible trace elements (see below).

255 We contend that if the concentrations of water in the melt inclusions have been compromised,
256 it is unlikely that these correlations would be preserved.

257 2. A main signature of the Gorgona komatiites is a spinifex texture that points towards the
258 exceptionally fast crystallization of the parental magma resulting in formation of skeletal
259 olivine. These olivine crystals contain very few melt inclusions and a search of >20,000
260 olivine fragments provided us with only a few tens of inclusions from ~ 30 μm to ~60 μm size
261 used in this and our previous studies (see respective phototables in [Kamenetsky et al., 2010](#)
262 and [Gurenko and Kamenetsky, 2011](#)). We contend that the studied fragments of skeletal
263 olivine containing melt inclusions formed during and shortly after emplacement of the
264 parental magma as a result of its rapid cooling, suggesting that there was virtually no time to
265 compromise H_2O concentrations in the included melts. Moreover, the observed wide
266 variations in H_2O in the studied melt inclusions (0.3–1.1 wt.%; see below), in contrast to
267 relatively narrow variations in forsterite content of the olivine hosts ($\text{Fo } 90.7 \pm 0.6$ mol.%,
268 excluding more evolved GOR94-17 komatiite and GOR94-32 picrite samples) would
269 additionally support the absence of post-entrapment H_2O re-equilibration, otherwise no H_2O -
270 range would have been preserved in the inclusions.

271 3. Formation of a spinifex texture requires not only rapid cooling of MgO -rich parental magma
272 but also the cooling must occur in a strong thermal gradient (7–35 $^\circ\text{C}/\text{cm}$; [Faure et al., 2006](#)).
273 If the parental magma ponded in a magma reservoir and had begun to crystallise olivine, the
274 thermal gradient is unlikely to have been strong enough, and the cooling too slow, to form
275 spinifex-textured olivine. All this argues against extensive olivine fractionation in a plumbing
276 system, where diffusive H_2O loss might occur. However unlike komatiites, the studied picrite
277 GOR94-32 is characterized by compositionally diverse olivine phenocrysts ($\text{Fo } 91.4 \pm 1.2$
278 mol.%), which show no skeletal appearance and contain abundant partially crystallised, glassy

279 inclusions. It is therefore possible that in contrast to komatiites, H₂O contents in melt
280 inclusions from this picrite sample could be strongly compromised.

281 4. An additional argument in support of the rapid quenching of komatiite parental magma could
282 be the presence of clusters of Cr-spinel crystals in the groundmass of the studied rocks. Many
283 of these spinel crystals, although extending to more Fe-rich compositions, are compositionally
284 similar to those included in olivine and exhibit no rims enriched in both ulvöspinel and
285 magnetite components (in contrast to what could be observed, if a host magma had a long
286 crystallization history; e.g., [Kamenetsky et al., 2001](#); [Gurenko et al., 2006](#)). Given that the
287 majority of olivine-hosted spinel inclusions are in the same growth zones of skeletal olivine
288 (as the melt inclusions), this suggests rapid crystallization of spinel occurred in the rising and
289 erupted magma along with its nearly simultaneous entrapment by growing olivine.

290 5. Partial loss of H₂O from inclusions during laboratory heating is possible and thus the
291 concentrations of H₂O in the included melts have to be considered as lower-end estimates.
292 However as noted by [Sobolev et al \(2016\)](#) in Archaean komatiites, melt inclusions with a
293 diameter >30 µm appear to preserve unbiased H₂O concentrations if magma was cooling fast
294 (while forming spinifex), as well as during laboratory heating. Moreover, the existing
295 significant correlations of H₂O with incompatible elements (see below) suggest that this
296 process is unlikely to have had a significant effect.

297
298 The present results of volatile analysis in the studied melt inclusions are listed in **Table**
299 **S2.2** (*Supporting online material*), along with the volatile concentrations, boron contents and
300 isotopic composition obtained by [Kamenetsky et al. \(2010\)](#) and [Gurenko and Kamenetsky](#)
301 [\(2011\)](#). The following observations can be made based on these data:

302

303 1. The concentrations of volatile components in the analysed melt inclusions (35–297 $\mu\text{g/g}$ CO_2 ,
304 0.26–1.11 wt.% H_2O , 67–107 $\mu\text{g/g}$ F, 556–879 $\mu\text{g/g}$ S and 186–304 $\mu\text{g/g}$ Cl) are in very good
305 agreement with our previously published data set. Correction for post entrapment
306 crystallization of olivine (14–38 wt.% Ol; **Table S2.2** – *Supporting online material*) results in
307 the following ranges: 26–222 $\mu\text{g/g}$ CO_2 , 0.2–0.83 wt.% H_2O , 52–86 $\mu\text{g/g}$ F, 431–730 $\mu\text{g/g}$ S
308 and 142–209 $\mu\text{g/g}$ Cl. Comparison of these ranges with those reported for chromite-hosted
309 melt inclusions by [Shimizu et al. \(2009\)](#) (up to 4000 $\mu\text{g/g}$ CO_2 and below 0.4 wt.% H_2O ,
310 except for one inclusion with 0.91 wt.% H_2O), reveals that almost all inclusions analysed in
311 the present study are characterised by significantly lower CO_2 concentrations but have higher
312 H_2O at an equivalent CO_2 (**Fig. 3a**).

313 2. Decompression degassing of magma results in preferential exsolution of CO_2 (as opposed to
314 H_2O) into vapour phase ([Dixon and Stolper, 1995](#)). The concentrations of H_2O and CO_2
315 directly measured by SIMS in the Gorgona melt inclusions reflect the last vapour-melt
316 equilibrium in the magmatic system for the time of eruption and thus represent a minimum
317 pressure of magma fractionation, as the melts could have been partially degassed. According
318 to the *VolatileCalc* solution model ([Newman and Lowenstern, 2002](#)), they correspond to H_2O -
319 CO_2 gas pressures between 5 and 30 MPa or to <1-km crustal depth (**Fig. 3a**).

320 3. Numerous studies ([Esposito et al., 2011](#); [Steele-Macinnis et al., 2011](#); [Hartley et al., 2014](#);
321 [Moore et al., 2015](#); [Wallace et al., 2015](#); [Mironov et al., 2015](#)) have demonstrated that 40 to
322 90% of the original CO_2 dissolved in the melt at the time of inclusion entrapment can be lost
323 to a shrinkage bubble during post-entrapment cooling. A correction algorithm described by
324 [Wallace et al. \(2015\)](#) was therefore used to reconstruct the original CO_2 and H_2O
325 concentrations in the included melts (see *Supporting online material*). These calculations
326 reveal that 79–92% (average 87%) of the original CO_2 and 1–5% (average 2%) of the original
327 H_2O have been lost to the shrinkage bubble, in agreement with the results of the above

328 studies. The following ranges of volatile concentrations were obtained after correction:
329 286–1748 $\mu\text{g/g}$ CO_2 , 0.2–0.86 wt.% H_2O , 48–82 $\mu\text{g/g}$ F, 398–699 $\mu\text{g/g}$ S and 132–198 $\mu\text{g/g}$
330 Cl. According to the *VolatileCalc* solution model (Newman and Lowenstern, 2002), these
331 results correspond to $\text{H}_2\text{O-CO}_2$ gas pressures between 20 and 200 MPa (average 86 ± 44 MPa,
332 1 SD; **Table S2.2** – *Supporting online material*) or to ~2.5-km crustal depth (**Fig. 3b**).

333 4. The concentrations of sulphur (either corrected for post entrapment crystallisation and
334 shrinkage bubble volatile exsolution or not) are lower than those of MORB and ocean island
335 basalt (OIB) submarine glasses (usually $S > 800$ $\mu\text{g/g}$ at ~7–10 wt.% FeO; Wallace and
336 Carmichael, 1992), but plot above the “sulphur saturation line” defined by compositions of
337 sulphide saturated experimental melts from Haughton et al. (1974) (**Fig. 4a**). The presence of
338 micron-scale sulphide globules inside several melt inclusions suggests saturation of the
339 included melts with sulphur. It is possible that this saturation might be caused by post-
340 entrapment loss of Fe from the inclusions (Danyushevsky et al., 2002). However, there is
341 good positive correlation of S with Ce ($R^2 = 0.77$ and 0.96 for uncorrected and corrected S
342 concentrations, respectively, except for one outlier; **Fig. 4b**), as well as significant
343 correlations of S with other incompatible elements [e.g., Ti (0.87), Sr (0.71), Zr (0.61), Ba
344 (0.47), La (0.54), Pr (0.67), Nd (0.49), Sm (0.42), Eu (0.64), Tb (0.77), Ho (0.58), Er (0.81),
345 Lu (0.56), Hf (0.53); the respective R^2 values for corrected S concentrations are given in
346 brackets]. Such relationships cannot be explained by either the later, post-entrapment origin of
347 sulphide phase in the inclusions or by magma contamination, but may imply incompatible
348 behaviour of S at an early stage of magma fractionation and probably undersaturation of high-
349 Mg “primary” magma with sulphur, as demonstrated on MORB magmas by Sobolev and
350 Hofmann (1999).

351 5. Similarly, H_2O concentrations (in particular, post-entrapment crystallisation- and shrinkage
352 bubble-corrected values) have a clear positive correlation with SiO_2 ($R^2 = 0.60$) (**Fig. 4c**) and

353 still significant negative correlations with some incompatible elements, such as Ti (0.50), Sr
354 (0.43), Y (0.43), Zr (0.54), Ce (0.44), Sm (0.79), Dy (0.49), Ho (0.73), Er (0.58), Tm (0.43),
355 Yb (0.74), Lu (0.46); the respective R^2 values are given in brackets (**Fig. 4d**).

356 6. There are, however, no correlations of H₂O with fluid mobile incompatible elements (e.g., Ba,
357 K), Pb and Th, also implying that H₂O, along with S, might have not been degassed during
358 magma fractionation at shallow depth. One possible explanation of the observed positive
359 correlation of H₂O with SiO₂ (**Fig. 4c**) could be incompatible behaviour of water during
360 magma fractionation. However, one would expect also a coherent increase in H₂O with
361 increasing concentrations of the other incompatible elements. As this is not the case, we
362 suggest that the correlation between SiO₂ and H₂O, in conjunction with negative trace
363 element-H₂O correlations, could be explained by a gradual increase in the degree of partial
364 melting of a clinopyroxene-depleted mantle source under hydrous conditions (e.g., [Parman
365 and Grove, 2004](#)). The coherent increase in SiO₂ and H₂O contents in the magma can be
366 explained by H₂O-fluxed decompression melting of refractory mantle accompanied by
367 increasing contribution of orthopyroxene to the melting reaction, and consequent progressive
368 depletion of trace element concentrations in the resulting melts.

369 7. The concentrations of chlorine in the included melts show no relationship with H₂O, CO₂ or S
370 (as well as the ratios of these volatile component concentrations to those of incompatible
371 elements, such as CO₂/Nb, H₂O/Ce, F/Zr, Cl/Nb, and S/Ce) but show a significant linear
372 correlation with fluorine ($R^2 = 0.43$ and 0.46 for uncorrected and corrected concentrations,
373 respectively) (**Fig. 4e**). Chlorine and fluorine usually behave as incompatible elements during
374 partial melting and magma fractionation, if their juvenile concentrations were not affected by
375 later degassing or contamination events (e.g., [Carroll and Webster, 1994](#); [Jambon, 1994](#)). The
376 observed F-Cl correlation may thus suggest that the reported F and Cl concentrations were not

377 influenced by degassing or contamination at crustal depth and are likely to reflect mantle
378 derived compositions, in agreement with incompatible behaviour of S and H₂O.

379

380 **5. Discussion**

381 *5.1. Message from oxygen isotopes*

382 Oxygen isotopes represent one of the most effective ways of tracing crustal components
383 in the source of mafic magmas and can provide robust constraints on shallow-level crustal
384 contamination because fractionation of oxygen isotopes is much more significant in low-
385 temperature hydrothermal processes, than in the mantle (e.g. [Kyser et al., 1987](#); [Woodhead et al.,](#)
386 [1993](#); [Eiler et al. 1995, 1996, 1997](#); [Garcia et al., 1998](#); [Harris et al., 2000, 2015](#); [Widom and](#)
387 [Farquhar 2003](#); [Bindeman et al. 2005, 2006, 2008](#); [Wang and Eiler, 2008](#); [Day et al., 2009](#);
388 [Martin et al., 2011](#); [Genske et al., 2013](#)). Oxygen isotope heterogeneity of the oceanic crust is
389 generally caused by seawater and/or seawater-derived fluid alteration (e.g., [Muehlenbachs et al.,](#)
390 [1974](#); [Hattori and Muehlenbachs, 1982](#); [Condomines et al., 1983](#); [Muehlenbachs 1986](#); [Alt et al.,](#)
391 [1986](#)). The oceanic crust can be affected by both low (<300–400°C) and relatively high
392 (>400°C) temperature fluid-rock interaction. It can vary in oxygen isotopic composition with
393 depth, mostly due to cross-over of oxygen isotopic fractionation factors (and their magnitude)
394 between minerals and water at ~300°C. Indeed, most of the oceanic crustal rocks altered by
395 seawater cover a ~10‰ range of $\delta^{18}\text{O}$ (from ~2–3‰ to ~11–13‰) spanning the “normal”- $\delta^{18}\text{O}$
396 mid-ocean ridge basalt (MORB) magma value of $\sim 5.6 \pm 0.2\text{‰}$ ([Gregory and Taylor, 1981](#); [Alt et](#)
397 [al., 1986](#); [Stakes and Taylor, 1992](#); [Bindeman, 2008](#); [Martin et al., 2011](#); [Yamaoka et al., 2012](#);
398 [Jacques et al., 2013](#) among others). But it is also never altered to $\delta^{18}\text{O}$ values lower than ~2‰ in
399 its middle and lower sections because $\Delta^{18}\text{O}_{\text{rock-water}}$ isotope fractionation is effectively $0 \pm 1\text{‰}$ at
400 high (>400°C) temperatures ([Gregory and Taylor 1981](#); [Stakes and Taylor 1992](#); [Bindeman,](#)
401 [2008](#); [Martin et al., 2011](#)). During subsequent subduction and recycling, the relative proportions

402 of ^{18}O -enriched and ^{18}O -depleted material has been shown to remain broadly similar to those in
403 the ocean crust prior to subduction, leading to $\delta^{18}\text{O}$ values in erupted volcanic-arc products that
404 are distinct from that of pristine mantle (e.g., [Bebout and Barton 1989](#); [Putlitz et al. 2000](#)).

405 Previous studies of tholeiitic to alkali basalts from Iceland, Hawaii, the islands of Tristan
406 da Cunha, Gough, Canary and Azores (e.g., [Harris et al., 2000](#); [Bindeman et al., 2008](#); [Wang and](#)
407 [Eiler, 2008](#); [Day et al., 2009](#); [Genske et al., 2013](#)) have demonstrated that a coherent decrease of
408 $\delta^{18}\text{O}_{\text{Ol}}$ and Fo is most likely to be a signature of assimilation of low- $\delta^{18}\text{O}$ crustal rocks by
409 ascending magma. This results in crystallization of olivine with lower than typical “mantle” (i.e.,
410 4.8–5.4‰) $\delta^{18}\text{O}$ values from hybrid magma. The slope of such Fo- $\delta^{18}\text{O}$ relationships may vary
411 significantly depending on the particular O-isotope composition of a contaminant, ranging from
412 the most extreme case of Hawaii ($\delta^{18}\text{O}_{\text{Ol}}$ decreases from 5.3‰ to 4.6‰ in the range from Fo₉₀ to
413 Fo₈₈ i.e., 0.35‰/mol.% Fo; [Wang and Eiler 2008](#)) through the Canaries (from 5.0‰ to 4.7‰ in
414 the range from Fo₈₄ to Fo₇₉, i.e. 0.06‰/mol.% Fo; [Day et al., 2009](#)) to the Azores ($\delta^{18}\text{O}_{\text{Ol}} =$
415 5.2–4.8‰ in olivines Fo_{90–77}, i.e., 0.03‰/mol.% Fo) (see *contamination trends* in **Fig. 2c**).
416 Conversely, olivine phenocrysts crystallized from mantle-derived magmas can show no clear
417 signs of shallow-depth crustal contamination (for example, Society, Samoa and Canary islands,
418 and the Karoo and Etendeka large igneous provinces). These olivine phenocrysts are
419 characterised by elevated $\delta^{18}\text{O}$ relative to typical upper mantle values and this was ascribed to
420 the presence of an ^{18}O -enriched component in the magma source (e.g., [Eiler et al., 1997](#);
421 [Gurenko et al., 2011](#); [Harris et al., 2015](#)).

422 To justify such trends, the analytical precision of a “single grain” O-isotope
423 determination must be at ± 0.1 – 0.2 ‰, 2 SD, and such values are typical for laser fluorination
424 analyses (e.g., [Bindeman, 2008](#)). In the case of SIMS measurements, one viable way to maintain
425 the required analytical precision is to increase a number of individual measurements within a
426 single grain. As noted above, most of the studied Gorgona olivine grains were multiply analysed

427 by SIMS. No substantial compositional difference has been recognised between internal and
428 external parts of the grains, except for the second subordinate maximum in the “rim” probability
429 density distribution curve at ~5.6‰ (**Fig. 2e**). As most of the studied olivine phenocrysts exhibit
430 varying degrees of serpentinisation but no clear relationship of Fo with $\delta^{18}\text{O}_{\text{OI}}$ (**Fig. 2c**), and
431 since shallow crustal contamination of the studied samples was not previously identified by
432 [Gurenko and Kamenetsky \(2011\)](#) nor by our present volatile data, our preferred explanation for
433 the second maximum and probably for the all $\delta^{18}\text{O}_{\text{OI}}$ values in excess of the “mantle” range is a
434 diffusive oxygen isotope exchange between olivine (4.8–5.4‰) and products of its low-
435 temperature alteration (for example, with serpentine with $\delta^{18}\text{O}$ up to ~13‰; [Martin et al., 2011](#)).

436 A less probable possibility is that the shift to more positive $\delta^{18}\text{O}$ olivine compositions
437 (**Fig. 2e**) could be related to admixture of a portion of a second magma derived from an ^{18}O -
438 enriched mantle component, or by analogy with [Martin et al. \(2011\)](#) who reported $\delta^{18}\text{O}$ values of
439 up to 6.1‰ in Mt. Shasta olivine phenocrysts, and related them to “a ^{18}O pre-enriched” peridotite
440 mantle wedge component. However, we consider this explanation unlikely mostly because (a)
441 the rapid, *in-situ* crystallisation (advocated herein) of skeletal olivine in the magma either en
442 route to the surface or later in the lava flow would result in more diffused distribution of $\delta^{18}\text{O}_{\text{OI}}$
443 values, with no well shaped maximums, as shown in **Fig. 2e**, and (b) the observed $\delta^{18}\text{O}$
444 enrichment is related to the edges of the studied olivine grains, which were in direct contact with
445 serpentine filling grain fractures and whose origin can be ascribed to later alteration stage of the
446 lava flows. In addition, a subordinate number of $\delta^{18}\text{O}$ -enriched compositions determined for
447 olivine “cores” (**Fig. 2e**) are ascribed to the so-called “3D-effect”, when ion beam visually
448 placed in the centre of a grain is in fact analysing its remaining outer part oriented parallel to the
449 sample surface.

450 Calculation the average “single grain” $\delta^{18}\text{O}_{\text{OI}}$ composition from all individual $\delta^{18}\text{O}_{\text{OI}}$
451 measurements performed for each olivine grain, regardless of whether they represented “core” or

452 “rim” areas, results in the average standard deviation of mean external reproducibility of
453 $\pm 0.12\%$, 2 SE (grain to grain range from ± 0.06 to $\pm 0.26\%$ due to the different number of
454 replicates), being comparable with those of single-grain laser fluorination. Figure 5 shows
455 averaged “within-grain” oxygen isotope compositions of the studied Gorgona olivines with no
456 discrimination between their internal and external zones. Like in **Fig. 2c**, no relationship between
457 Fo contents and $\delta^{18}\text{O}_{\text{Ol}}$ values for olivines can be observed for komatiite lavas. In contrast,
458 olivines from picrite GOR94-32 show a subtle positive correlation ($R = 0.53$), best approximated
459 by a polynomial quadratic equation (**Fig. 5a**), which is significant at 95% confidence level
460 (critical value of the Pearson correlation coefficient R is 0.44 at $N = 20$). Similarly, as in **Fig. 2e**,
461 the probability density distribution curves reveal a common maximum of typical mantle $\delta^{18}\text{O}_{\text{Ol}}$
462 values between 5.2 and 5.3‰ (**Fig. 5b**). A subordinate peak at $\sim 5.6\%$ for olivines from
463 komatiites and three less-pronounced subordinate peaks at $\sim 5.6\text{--}5.9\%$ for olivines from picrite
464 are thought to have been inherited from the analyses of rims.

465 If our assumption about the possible impact of later serpentinisation on the O-isotope
466 composition of olivine is correct, then some of the $\delta^{18}\text{O}_{\text{Ol}}$ values, including those from the
467 “mantle” range, could have been systematically shifted to more ^{18}O -enriched compositions. This
468 would result in more diffused shape of the maximums in the density distribution (**Fig. 2e**) and
469 representing the upper level of $\delta^{18}\text{O}_{\text{Ol}}$ estimates. Moreover, the absence of a clear relationship
470 between Fo content and $\delta^{18}\text{O}_{\text{Ol}}$ in komatiites also could be explained by this olivine-serpentine
471 O-isotope exchange, during which the isotopic composition of olivine was modified to a greater
472 extent than the Fo content (as serpentinisation does not affect forsterite number in olivine, as
473 recently shown by [Birner et al., 2016](#)). In this context, the most Fo-rich olivines of the “picrite”
474 trend in **Fig. 5a** having $\delta^{18}\text{O}_{\text{Ol}}$ values outside “mantle” range could be affected by this
475 serpentinisation process, suggesting also that their former unmodified $\delta^{18}\text{O}_{\text{Ol}}$ values originally
476 corresponded to the “normal” mantle $\delta^{18}\text{O}_{\text{Ol}}$ range.

477

478 *5.2. Evidence against crustal contamination*

479 The parental magmas of komatiites are hotter, up to 1600°C for Archaean komatiites
480 (e.g., Herzberg et al., 2007 and references therein), as compared to MORB and OIB magmas,
481 and therefore are more likely to melt and assimilate surrounding wall rocks en route to the
482 surface. A melt inclusion study of 2.7-Ga-old Belingwe komatiites, Zimbabwe, demonstrated
483 that their parental magmas probably contained up to 1 wt.% H₂O, but the source of water was
484 uncertain (i.e., shallow magma contamination versus melting of a hydrous mantle plume source;
485 e.g., Shimizu et al., 2001; Berry et al., 2008; Kent et al., 2009). Recently, Sobolev et al. (2016)
486 reported marked H₂O enrichment of Archaean komatiites from the Abitibi greenstone belt,
487 Canada, with H₂O/Ce >6000, and proposed the presence of a hydrous, deep mantle reservoir
488 formed early in the Earth's history. However, those melts with high Cl/K₂O ≈ 7, Cl/F ≈ 100 and
489 Cl/H₂O ≈ 0.6 ratios were explained by Sobolev et al. (2016) as being due to assimilation of
490 serpentinites altered by seawater with possible involvement of seawater-derived brines. For
491 comparison, Cl/K₂O from 0.23 to 0.65, Cl/F from 2.4 to 3.5, and Cl/H₂O from 0.02 to 0.09 in the
492 studied Gorgona melt inclusions are well below the above values ascribed to contamination by
493 Sobolev et al. (2016), and the controversy remains as to whether the obtained volatile
494 concentrations preserved in the Gorgona melt inclusions are pristine or they were inherited
495 during assimilation of crustal rocks by the magma (e.g., Shimizu et al., 2001; Berry et al., 2008;
496 Kent et al., 2009; Kamenetsky et al., 2010).

497 One of the main arguments against a hydrous origin of the Gorgona komatiites is their
498 extreme depletion in incompatible trace elements. This depletion becomes progressively more
499 pronounced on going from basalts through komatiites to picrites. However, it is clear that all
500 these rock types are related to a similar type of depleted mantle source (e.g., Arndt et al., 1997;
501 Révillon et al., 2000, 2002). These authors ascribed the origin of volatiles (and in particular

502 water) either to sub-solidus alteration processes or to assimilation of hydrated crust in a shallow-
503 level magma reservoir. This latter conclusion was also reached by Shimizu et al. (2009), who in
504 their study of chromites from the beach sands of Gorgona described CO₂-rich (40–4000 µg/g)
505 melt inclusions with highly variable H₂O (0.03–0.9 wt. %) and Cl (6–1056 µg/g) and proposed
506 that the concentrations of volatile components, and especially Cl, were influenced by magma
507 degassing or interaction with seawater or brine prior to entrapment.

508 Significantly, however, Gurenko and Kamenetsky (2011), who studied boron contents
509 and B isotopic compositions in the same melt inclusions analysed during the present study,
510 argued that it was not possible to unequivocally prove magma contamination only on the basis of
511 Cl/K₂O vs. H₂O/K₂O relationships (or similar, where Cl- and H₂O-concentrations are normalised
512 to a concentration of an incompatible element). These authors showed that although H₂O/K₂O-
513 Cl/K₂O or H₂O/K₂O-B/K₂O systematics can be explained by contamination of magma by
514 seawater or NaCl-rich brines, the relationships between B/K₂O and Cl/K₂O or B/K₂O and δ¹¹B,
515 for the same inclusions do not support their role, as well as a role of altered oceanic crust,
516 serpentinites or marine sediments as possible contaminants.

517 The highest obtained H₂O/Ce = 4490 of the studied melt inclusions is significantly lower
518 than that of the Archaean komatiites (H₂O/Ce >6000; Sobolev et al., 2016) and the highest
519 CO₂/Nb = 3320 and Zr/Y = 2.1 are very close to, but F/Zr = 2.6 is significantly lower than, those
520 of the “primary komatiite” of Shimizu et al. (2009) (i.e., CO₂/Nb = 4000 ± 2200, F/Zr = 7.0 ±
521 1.7, Zr/Y = 1.7 ± 0.3). In addition to not being as high as in this hypothetical “primary
522 komatiite”, the F/Zr ratios (1.5–2.6) in the olivine melt inclusions analysed in this study, are at
523 the lower end of the F/Zr range in the chromite-hosted inclusions of Shimizu et al. (2009). We
524 note that all chromites studied by Shimizu et al. (2009) are from the beach sands and are likely to
525 come from any type of mafic rocks exposed on Gorgona, not necessarily from komatiites. This
526 may suggest that the inclusions analysed during the present study and those of Shimizu et al.

527 (2009) perhaps represent two similar but quite different magmatic systems, at least with respect
528 to their dissolved volatiles.

529 The observed significant correlations of S, and to a lesser extent H₂O, with almost all
530 highly incompatible elements (**Fig. 4b, d**), the good correlation between F and Cl (**Fig. 4e**), in
531 addition to there being no clear relationship between Cl and H₂O, suggest that neither shallow
532 magma degassing nor crustal contamination have affected volatile concentrations in the studied
533 magmas during ascent.

534 Moreover, if rapid crystallization of skeletal olivine occurred at shallow crustal depth (no
535 deeper than ~2.5 km, as follows from CO₂-H₂O data) during magma transport to the surface and
536 probably continued *in-situ* in the lava flow, in contrast to the much slower crystallization in a
537 magma chamber, then H₂O (as well as chlorine and probably other volatiles) must have been
538 supplied to the magma by interaction with near-surface, seawater pre-conditioned crustal rocks.
539 This would imply crystallization of olivine with higher than “normal mantle” $\delta^{18}\text{O}$ composition
540 (i.e., 4.8–5.4‰), because upper-level crustal rocks suffered low-temperature (<300 °C) alteration
541 by seawater are characterized by elevated, up to 13‰, $\delta^{18}\text{O}$ values (see above). Since the
542 majority of the studied olivines are “mantle”-like in respect of $\delta^{18}\text{O}$, we consider the possibility
543 of surface contamination of the komatiite parental magma by variable amount of seawater-
544 preconditioned crustal components as unlikely.

545

546 5.4. Boron vs. oxygen isotope relationships

547 Boron vs. oxygen isotope systematics have been shown to be a very powerful tool in
548 discriminating between pure mantle melting and crust recycling, slab-mantle wedge interaction
549 or shallow depth magma contamination. In particular, [Chaussidon and Jambon \(1994\)](#),
550 [Chaussidon and Marty \(1995\)](#), [Smith et al. \(1995\)](#) have demonstrated on primitive MORB and
551 OIB glasses that positive $\delta^{11}\text{B}$ associated with increasing oxygen isotope ($\delta^{18}\text{O} > 5.5\text{‰}$) and

552 radiogenic Sr isotope ratios are more likely to result from shallow-level assimilation of oceanic
553 crust, whereas negative $\delta^{11}\text{B}$ values accompanied by low $\delta^{18}\text{O} < 5.5\%$ point towards interaction
554 of primitive magmas with the Layer 3 gabbroic crust. Moreover, the systematically higher $\delta^{11}\text{B}$,
555 reported for arc lavas by [Peacock and Hervig \(1999\)](#), as compared to exhumed subduction
556 related metamorphic rocks, may suggest that dehydration reactions can significantly decrease
557 $\delta^{11}\text{B}$ of the subducting oceanic crust and sediments, thereby implying significant fractionation of
558 ^{11}B and ^{10}B and enrichment of the fluid in ^{11}B isotope.

559 Although variable but generally positive $\delta^{11}\text{B}$ values have been identified in mantle
560 wedge serpentinites at the slab-mantle interface (e.g., [Benton et al., 2001](#); [Savov et al., 2005](#),
561 [2007](#)), it has also been shown that subduction-related serpentinites, eclogites and slab-derived
562 melts may be strongly depleted in ^{18}O , and have significantly lower $\delta^{18}\text{O}$ than that of typical
563 mantle (down to $\sim 2\text{--}4\%$) (e.g., [Bindeman et al., 2005](#); [Bindeman 2008](#); [Martin et al., 2011](#);
564 [Jacques et al., 2013](#)). In addition, [Martin et al. \(2011\)](#) have demonstrated that slab-derived fluids
565 can be markedly enriched in ^{18}O , if dehydration occurred at low T , i.e., $< 300^\circ\text{C}$. This is because
566 the fluid-rock O-isotope fractionation factor, $\Delta^{18}\text{O}_{\text{fluid-rock}}$, can be as high as 10% at this
567 temperature. But O-isotope composition of the fluid can broadly correspond to the composition
568 of the source rock if released at higher temperatures (because $\Delta^{18}\text{O}_{\text{fluid-rock}} \approx 0$ at $T > 400^\circ\text{C}$).

569 [Gurenko and Kamenetsky \(2011\)](#) previously identified two groups of Gorgona olivine-
570 hosted melt inclusions in B- $\delta^{11}\text{B}$ space. The first group of inclusions has relatively low $\delta^{11}\text{B}$
571 from -11.5 to -7.3% (average $-9.0 \pm 1.5\%$), spanning the entire range of B concentrations and
572 closely corresponding to the Earth's mantle value of $-10 \pm 2\%$ ([Chaussidon and Marty, 1995](#)).
573 The second group is characterised by generally higher $\delta^{11}\text{B}$ values than mantle $\delta^{11}\text{B}$ (up to
574 $+15.6\%$) and increasing B concentrations up to $1.6 \mu\text{g/g}$ (see Fig. 3 in [Gurenko and](#)
575 [Kamenetsky, 2011](#)). The first group was interpreted to be of mantle origin, whereas the second
576 was explained by input of $< 3 \text{ wt.}\%$ of ^{11}B -enriched (possibly subduction related) fluid into the

577 source of the Gorgona komatiites. The main limitation of the proposed mechanism, however, is
578 the absence of a clear geochemical signature of subduction in the composition of the studied melt
579 inclusions such as depletion of high field strength elements (Nb, Zr, Ti) coupled with U-shaped
580 patterns of incompatible element spectra due to the enrichment of large ion lithophile elements
581 (Rb, Ba, K, Sr) and Pb. It is important to note that a similar absence of the subduction signatures
582 in the H₂O-rich olivine-hosted melt inclusions from the 2.7-billion-year-old komatiites from the
583 Abitibi greenstone belt in Canada led [Sobolev et al \(2016\)](#) to propose the presence of a hydrous
584 deep-mantle reservoir in the Archaean mantle.

585 Figure 6 shows the B isotopic composition of Gorgona melt inclusions from [Gurenko and](#)
586 [Kamenetsky \(2011\)](#) linked with new O-isotopic data on the hypothetical melts in equilibrium
587 with olivines, for which $\delta^{18}\text{O}_{\text{Ol}}$ were determined (olivine equivalent). In order to calculate the O
588 isotope fractionation factor we used a coefficient $A = -0.54$ in the general isotope fractionation
589 equation:

590

$$591 \quad \Delta^{18}\text{O}_{\text{Ol-melt}} = A \times 10^6/T^2 \quad \text{Eq. 1}$$

592

593 defined for komatiite by [Matthews et al. \(1998\)](#). The calculated $\Delta^{18}\text{O}_{\text{Ol-melt}}$ was found to be
594 between -0.199 and -0.212 in the T -range of 1320 – 1380 °C, i.e., the crystallization temperatures
595 of the studied olivines ([Kamenetsky et al., 2010](#)). Surprisingly, but even with a large range of
596 boron isotopic composition from -11.5 to 15.6 ‰ of $\delta^{11}\text{B}$, the assigned $\delta^{18}\text{O}_{\text{melt}}$ values only
597 slightly exceed the “mantle” interval, ranging from 5.0 to 5.9 ‰, whilst the inclusions of the first,
598 low- $\delta^{11}\text{B}$ group of [Gurenko and Kamenetsky \(2011\)](#) fit almost entirely the “mantle” array in
599 respect of both O and B isotope systematics (**Fig. 6**).

600 Although the mantle origin of the first, low- $\delta^{11}\text{B}$ group of inclusions can be determined
601 on the basis of combined $\delta^{11}\text{B}$ - $\delta^{18}\text{O}$ isotopic data, the origin of the second group of inclusions

602 with varying $\delta^{11}\text{B}$ data remains enigmatic. We have calculated several two-component mixing
603 trends in $\delta^{18}\text{O}$ - $\delta^{11}\text{B}$ space (**Fig. 6**), illustrating the effects of possible interaction of fluids
604 released from oceanic crust at different temperatures, with a MORB-like depleted mantle source,
605 as well as the effects of the possible presence of recycled crust and variously dehydrated
606 serpentinite in the magma source cf. [Gurenko and Kamenetsky \(2011\)](#). We used B contents and
607 $\delta^{11}\text{B}$ values of the mixing end-members as defined by [Gurenko and Kamenetsky \(2011\)](#) coupled
608 with the respective oxygen isotope data (for explanation see **Table S2.3** – *Supporting online*
609 *material*). As shown by the calculations, our new B-O isotopic data also confirm the importance
610 of a H_2O - and B-rich fluid component released at low T (*FL1*) and/or serpentinite (*SERP1*)
611 interacting with mantle source rocks (less than 5% of input is required) and, in contrast,
612 demonstrate the unlikely, but still possible, role of the recycled crust (*REC*), dehydrated
613 serpentinite (*SERP2*) and fluids released at greater depths and higher temperatures (*FL2* and
614 *FL3*) (more than 10% addition to the source is required). However, we note that although the
615 potential role of each of the selected mixing end-members cannot be completely ruled out taking
616 into account the analytical precision of $\delta^{11}\text{B}$ and $\delta^{18}\text{O}$ determinations, their possible admixture to
617 the *MANT* source should not significantly affect the volatile concentrations of the resulting melts
618 as no difference in volatile contents exists between high- $\delta^{11}\text{B}$ and low- $\delta^{11}\text{B}$ groups of inclusions.

619 However, the question exists as to whether the Gorgona picrites and komatiites came
620 from a distinct or a compositionally similar mantle source. As noted by [Kerr et al. \(1996\)](#), in
621 addition to the difference in major and trace element ratios (e.g., Al/Ti, Ce/Sm, Gd/Yb), they
622 also show a subtle difference in their radiogenic isotope signatures, suggesting that their mantle
623 source is unlikely to be the same. Similar conclusions also can be derived from the two distinct
624 trends of magma fractionation in the Fo-NiO diagram (**Fig. 2b**). As shown by several recent
625 studies, Ni concentration in olivine (along with Mn and Ca) is a very good proxy to access
626 relative contribution of the peridotite (mantle) and pyroxenite (recycled crust) components in the

627 mantle source of primary magmas, and these relative contributions can be directly related to the
628 radiogenic isotope composition of the host lavas (e.g., [Sobolev et al., 2007, 2008](#); [Gurenko et al.,](#)
629 [2013](#), among others). Using the [Sobolev et al. \(2008\)](#) parameterisation for Ni in olivine, we
630 obtain substantially different fractions of anticipated pyroxenite-derived melt in the picritic (X_{pxm}
631 $= 0.27 \pm 0.07$, 1 SD) and “komatiitic” ($X_{pxm} = 0.40 \pm 0.06$, 1 SD) primary melts that also may
632 partially account for the observed subtle difference in oxygen and radiogenic isotope
633 compositions. Further implications of this method for the possible variability in mineral,
634 chemical and isotopic compositions of these types of rocks are beyond the scope of the present
635 paper. However, given that clinopyroxene is a major inventory of H₂O as, for instance, in the
636 depleted, MORB-like mantle (e.g., [Danyushevsky et al., 2000](#)), differences in pristine
637 concentrations of H₂O in Gorgona picrite and “komatiite” parental magmas (where komatiites
638 are more H₂O-rich) can be predicted.

639

640 **6. Conclusions**

- 641 1. The $\delta^{18}\text{O}$ values in the studied olivines from one picrite and five komatiites of Gorgona,
642 Colombia, range from 4.7 to 6.0‰, with the majority (~66% population) being within the
643 typical “mantle” olivine range of 4.8–5.4‰, but with a subordinate but still significant
644 number (~33% population) above, and only 2 olivine grains below, this range. No zoning or
645 systematic difference in forsterite contents and $\delta^{18}\text{O}_{\text{Ol}}$ values between the internal and
646 external parts of the grains have been recognised.
- 647 2. The probability density distribution curves reveal a common maximum of $\delta^{18}\text{O}_{\text{Ol}}$ at ~5.3‰ for
648 both internal and external zones of olivine, but the “rims” exhibit also an additional,
649 subordinate maximum at ~5.6‰ probably due to diffusive oxygen isotope exchange between
650 fresh and low-temperature alteration domains in the olivines. The O-isotope mantle signature
651 of the majority of the studied olivines do not support shallow depth contamination of the

652 Gorgona high-Mg magmas, and rather favour a deep mantle origin of high volatile
653 concentrations in the olivine-hosted melt inclusions.

654 3. The concentrations of volatile components in olivine-hosted melt inclusions analysed during
655 the present study agree well with our previously reported data. After correction for post-
656 entrapment crystallization of olivine in the inclusions upon cooling, the concentrations of CO₂
657 and H₂O reveal minimum pressure estimates of 5–30 MPa, which likely indicate the last
658 vapour-melt equilibrium shortly prior to eruption of magma (<1 km crustal depth). However,
659 ~87% and ~2% of the original CO₂ and H₂O, respectively, have been lost to the inclusion
660 shrinkage bubbles during magma cooling. After correction for this effect, the obtained
661 presumable undegassed ranges of volatile concentrations imply a H₂O-CO₂ gas pressure of 86
662 ± 44 MPa or ~2.5 km of crustal depth of olivine crystallisation.

663 4. Significant correlations of S and, to a lesser extent of H₂O, with a number of highly
664 incompatible elements, along with the correlation between F and Cl, but no clear relationship
665 of H₂O with Cl, argue against shallow depth degassing and/or crustal contamination of the
666 studied magmas.

667 5. The new B-O isotopic data confirm the importance of a H₂O- and B-rich fluid component
668 interacting with the source rocks of the Gorgona magmas, but reduce the likelihood of a role
669 for recycled crust and serpentinite. Therefore, the results of this study suggest that the
670 reported enrichment of volatile components and boron represent a deep mantle signature of
671 the studied Gorgona mafic and ultramafic magmas.

672

673 **Acknowledgments**

674 We thank Olivier Royer (*Service Commun de Microscopie Électronique et de Microanalyses,*
675 *Université de Lorraine*) for technical assistance during electron microprobe analyses, and Alex
676 Sobolev for fruitful discussions. The insightful reviews of Sally A. Gibson and two anonymous

677 referees helped us to improve the manuscript. Editorial handling of the paper by Michael J.
678 Bickle is gratefully acknowledged. The Museum of Natural History, Washington, DC, kindly
679 provided us with the standards for EPMA. All analytical costs were covered by CRPG (AAG's
680 internal funds). This is CRPG contribution number 24xx.

681

682

683 **References**

- 684 Allègre, C.J., 1982. Genesis of Archean komatiites in a wet ultramafic subducted plate. In:
685 Arndt, N., Nisbet, E.G. (Eds.) Komatiites. Berlin, Springer-Verlag, 495–500.
- 686 Alt, J.C., Muehlenbachs, K., Honnorez, J. 1986. An oxygen isotopic profile through the upper
687 kilometer of the oceanic crust, DSDP Hole 504B. *Earth and Planetary Science Letters* 80,
688 217–229.
- 689 Arndt, N.T., Nisbet, E.G., 1982. Komatiites. Fifth Edition, George Allen and Unwin, London,
690 pp. 526.
- 691 Arndt, N.T., Kerr, A.C., Tarney, J., 1997. Dynamic melting in plume heads: The formation of
692 Gorgona komatiites and basalts. *Earth and Planetary Science Letters* 146, 289–301.
- 693 Arndt, N., Ginibre, C., Chauvel, C., Albarède, F., Cheadle, M., Herzberg, C., Jenner, G., Lahaye,
694 Y., 1998. Were komatiites wet? *Geology* 26, 739–742.
- 695 Aitken, B.G., Echeverría, L.M., 1984. Petrology and geochemistry of komatiites and tholeiites
696 from Gorgona Island, Colombia. *Contributions to Mineralogy and Petrology* 86, 94–105.
- 697 Bebout, G.E., Barton, M.D., 1989. Fluid flow and metasomatism in a subduction zone
698 hydrothermal system: Catalina Schist terrane, California. *Geology* 17, 976–980.
- 699 Benton, L.D., Ryan, J.G., Tera, F., 2001. Boron isotope systematics of slab fluids as inferred
700 from a serpentine seamount, Mariana forearc. *Earth and Planetary Science Letters* 187,
701 273–282.
- 702 Berry, A.J., Danyushevsky, L.V., O'Neill, H.St.C., Newville, M., Sutton, S.R., 2008. Oxidation
703 state of iron in komatiitic melt inclusions indicates hot Archaean mantle. *Nature* 455,
704 960–963.
- 705 Bickle, M.J., Ford, C.E., Nisbet, E.G., 1977. The petrogenesis of peridotitic komatiites: evidence
706 from high-pressure melting experiments. *Earth and Planetary Science Letters* 37, 97–106.
- 707 Bindeman, I., 2008. Oxygen isotopes in mantle and crustal magmas as revealed by single crystal
708 analysis. In: Putirka, K.D., Tepley III, F.J. (Eds.) *Minerals, Inclusions and Volcanic
709 Processes*. *Rev. Mineral. Geochem.* 69, Mineral. Soc. Am., Washington DC, pp 445–478.
- 710 Bindeman, I.N., Eiler, J.M., Yogodzinski, G.M., Tatsumi, Y., Stern, C.R., Grove, T.L.,
711 Portnyagin, M., Hoernle, K., Danyushevsky, L.V., 2005. Oxygen isotope evidence for slab

712 melting in modern and ancient subduction zones. *Earth and Planetary Science Letters* 235,
713 480–496.

714 Bindeman, I.N., Sigmarsson, O., Eiler, J.M., 2006. Time constraints on the origin of large
715 volume basalts derived from O-isotope and trace element mineral zoning and U-series
716 disequilibria in the Laki and Grímsvötn volcanic system. *Earth and Planetary Science Letters*
717 245, 245–259.

718 Bindeman, I.N., Gurenko, A.A., Sigmarsson, O., Chaussidon, M., 2008. Oxygen isotope
719 heterogeneity and disequilibria of olivine phenocrysts in large volume basalts from Iceland:
720 evidence for magmatic digestion and erosion of Pleistocene hyaloclastites. *Geochimica et*
721 *Cosmochimica Acta* 72, 4397–4420.

722 Birner, S.K., Warren, J.M., Cottrell, E., Davis, F.A., 2016. Hydrothermal alteration of seafloor
723 peridotites does not influence oxygen fugacity recorded by spinel oxybarometry. *Geology* 44,
724 535–538.

725 Campbell, I.H., Griffiths, R.W., Hill, R.I., 1989. Melting in an Archaean mantle plume: heads it's
726 basalts, tails it's komatiites. *Nature* 339, 697–699.

727 Carroll, M.R., Webster, J.D., 1994. Solubilities of sulfur, noble gases, nitrogen, chlorine, and
728 fluorine in magmas. In: Carroll, M.R., Holloway, J.R. (Eds.) *Volatiles in magmas*. *Rev.*
729 *Mineral.* 30, Mineral. Soc. Am., Washington DC, pp 231–279.

730 Chaussidon, M., Jambon, A., 1994. Boron content and isotopic composition of oceanic basalts:
731 geochemical and cosmochemical implications. *Earth and Planetary Science Letters* 121,
732 277–291.

733 Chaussidon, M., Marty, B., 1995. Primitive boron isotope composition of the mantle. *Science*
734 269, 383–386.

735 Chiba, H., Chacko, T., Clayton, R.N., Goldsmith, J.R., 1989. Oxygen isotope fractionations
736 involving diopside, forsterite, magnetite, and calcite: application to geothermometry.
737 *Geochimica et Cosmochimica Acta* 53, 2985–2995.

738 Clague, D.A., Moore, J.G., Dixon, J.E., Friesen, W.B., 1995. Petrology of submarine lavas from
739 Kilauea's Puna Ridge, Hawaii. *Journal of Petrology* 36, 299–349.

740 Condomines, M., Grönvold, K., Hooker, P.J., Muehlenbachs, K., O'Nions, R.K., Óskarsson, N.,
741 Oxburgh, E.R., 1983. Helium, oxygen, strontium and neodymium isotopic relationships in
742 Icelandic volcanics. *Earth and Planetary Science Letters* 66, 125–136.

743 Danyushevsky, L.V., Eggins, S.M., Falloon, T.J., Christie, D.M., 2000. H₂O abundance in
744 depleted to moderately enriched mid-ocean ridge magmas; Part I: Incompatible behaviour,
745 implications for mantle storage, and origin of regional variations. *Journal of Petrology* 41,
746 1329–1364.

747 Danyushevsky, L.V., McNeill, A.W., Sobolev, A.V., 2002. Experimental and petrological
748 studies of melt inclusions in phenocrysts from mantle-derived magmas: an overview of
749 techniques, advantages and complications. *Chemical Geology* 183, 5–24.

750 Day, J.M.D., Pearson, D.G., Macpherson, C.G., Lowry, D., Carracedo, J.-C., 2009. Pyroxenite-
751 rich mantle formed by recycled oceanic lithosphere: oxygen-osmium isotope evidence from
752 Canary Island lavas. *Geology* 37, 555–558.

753 Dietrich, V.J., Gansser, A., Sommerauer, J., Cameron, W.E., 1981. Palaeogene komatiites from
754 Gorgona Island, East Pacific – A primary magma for ocean floor basalts? *Geochemical*
755 *Journal* 15, 141–161.

756 Dixon, J.E., Stolper E.M. 1995. An experimental study of water and carbon dioxide solubilities
757 in mid-ocean ridge basaltic liquids. Part II: Applications to degassing. *Journal of Petrology*
758 36, 1633–1646.

759 Dixon, J.E., Clague, D.A., Wallace, P., Poreda, R., 1997. Volatiles in alkalic basalts from the
760 North Arch Volcanic Field, Hawaii: Extensive degassing of deep submarine-erupted alkalic
761 series lavas. *Journal of Petrology* 38, 911–939.

762 Echeverría, L.M., 1980. Tertiary or Mesozoic komatiites from Gorgona island, Colombia: field
763 relations and geochemistry. *Contributions to Mineralogy and Petrology* 73, 253–266.

764 Echeverría, L.M., Aitken, B.G., 1986. Pyroclastic rocks: Another manifestation of ultramafic
765 volcanism on Gorgona Island, Colombia. *Contributions to Mineralogy and Petrology* 92,
766 428–436.

767 Eiler, J.M., 2001. Oxygen isotope variations in basaltic lavas and upper mantle rocks. In: Valley,
768 J.W., Cole, D.R. (Eds.) *Stable Isotope Geochemistry*. Rev. Mineral. Geochem. 43, Mineral.
769 Soc. Am., Washington DC, pp 319–364.

770 Eiler, J.M., Farley, K.A., Valley, J.W., Stolper, E.M., Hauri, E.H., Craig, H., 1995. Oxygen
771 isotope evidence against bulk recycled sediment in the mantle sources of Pitcairn Island
772 lavas. *Nature* 377, 138–141.

773 Eiler, J.M., Farley, K.A., Valley, J.W., Hofmann, A.W., Stolper, E.M., 1996. Oxygen isotope
774 constraints on the sources of Hawaiian volcanism. *Earth and Planetary Science Letters* 144,
775 453–468.

776 Eiler, J.M., Farley, K.A., Valley, J.W., Hauri, E., Craig, H., Hart, S.R., Stolper, E.M., 1997.
777 Oxygen isotope variations in ocean island basalt phenocrysts. *Geochimica et Cosmochimica*
778 *Acta* 61, 2281–2293.

779 Esposito, R., Bodnar, R.J., Danyushevsky, L.V., De Vivo, B., Fedele, L., Hunter, J., Lima, A.,
780 Shimizu, N., 2011. Volatile evolution of magma associated with the Solchiaro eruption in
781 the Phlegrean Volcanic District (Italy). *Journal of Petrology* 52, 2431–2460.

782 Faure, F., Arndt, N., Libourel, G., 2006. Formation of spinifex texture in komatiites: an
783 experimental study. *Journal of Petrology* 47, 1591–1610.

784 Gansser, A., 1950. Geological and petrological notes on Gorgona island in relation to north-west
785 S America. *Schweizerische Mineralogische und Petrographische Mitteilungen* 30, 219–237.

786 Gansser, A., Dietrich, V.J., Cameron, W.E., 1979. Palaeogene komatiites from Gorgona Island.
787 *Nature* 278, 545–546.

788 Garcia, M.O., Ito E., Eiler, J.M., Pietruszka, A.J., 1998. Crustal contamination of Kilauea
789 volcano magmas revealed by oxygen isotope analyses of glass and olivine from Puu Oo
790 eruption lavas. *Journal of Petrology* 39, 803–817.

791 Genske, F.S., Beier, C., Haase, K.M., Turner, S.P., Krumm, S., Brandl, P.A. 2013. Oxygen
792 isotopes in the Azores islands: crustal assimilation recorded in olivine. *Geology* 41, 491-
793 494.

794 Gregory, R.T., Taylor, H.P., 1981. An oxygen isotope profile in a section of Cretaceous oceanic
795 crust, Samail Ophiolite, Oman: evidence for $\delta^{18}\text{O}$ buffering of the oceans by deep (>5 km)

796 seawater-hydrothermal circulation at mid-ocean ridges. *Journal of Geophysical Research* 86,
797 2737–2755.

798 Grove, T.L., Parman, S.W., 2004. Thermal evolution of the Earth as recorded by komatiites.
799 *Earth and Planetary Science Letters* 219, 173–187.

800 Gurenko, A.A., Kamenetsky, V.S., 2011. Boron isotopic composition of olivine-hosted melt
801 inclusions from Gorgona komatiites, Colombia: New evidence supporting wet komatiite
802 origin. *Earth and Planetary Science Letters* 312, 201–212.

803 Gurenko, A.A., Hoernle, K.A., Hauff, F., Schmincke, H.-U., Han, D., Miura, Y.N., Kaneoka, I.,
804 2006. Major, trace element and Nd-Sr-Pb-O-He-Ar isotope signatures of shield stage lavas
805 from the central and western Canary Islands: Insights into mantle and crustal processes.
806 *Chemical Geology* 233, 75-112.

807 Gurenko, A.A., Bindeman, I.N., Chaussidon, M., 2011. Oxygen isotope heterogeneity of the
808 mantle beneath the Canary Islands: insights from olivine phenocrysts. *Contributions to*
809 *Mineralogy and Petrology* 162, 349–363.

810 Gurenko, A.A., Geldmacher, J., Hoernle, K.A., Sobolev, A.V., 2013. A composite, isotopically-
811 depleted peridotite and enriched pyroxenite source for Madeira magmas: Insights from
812 olivine. *Lithos* 170–171, 224–238.

813 Harris, C., Smith, H.S., le Roex, A.P., 2000. Oxygen isotope composition of phenocrysts from
814 Tristan da Cunha and Gough Island lavas: variation with fractional crystallization and
815 evidence for assimilation. *Contributions to Mineralogy and Petrology* 138, 164–175.

816 Harris, C., Roux, P., Cochrane, R., Martin, L., Duncan, A.R., Marsh, J.S. Roex, A.P., Class, C.,
817 2015. The oxygen isotope composition of Karoo and Etendeka picrites: High $\delta^{18}\text{O}$ mantle or
818 crustal contamination? *Contributions to Mineralogy and Petrology* 170, 1–24.

819 Hartley, M.E., MacLennan, J., Edmonds, M., Thordarson, T., 2014. Reconstructing the deep CO_2
820 degassing behaviour of large basaltic fissure eruptions. *Earth and Planetary Science Letters*
821 393, 120–131.

822 Hattori, K., Muehlenbachs, K., 1982. Oxygen isotope ratios of the Icelandic crust. *Journal of*
823 *Geophysical Research* 87, 6559–6565.

824 Haughton, D.R., Roeder, P.L., Skinner, B.J., 1974. Solubility of sulfur in mafic magmas.
825 *Economic Geology* 69, 541–567.

826 Herzberg, C., 1995. Generation of plume magmas through time: an experimental perspective.
827 *Chemical Geology* 126, 1–16.

828 Herzberg, C., Asimow, P.D., Arndt, N., Niu, Y., Leshner, C.M., Fitton, J.G., Cheadle, M.J.,
829 Saunders, A.D., 2007. Temperatures in ambient mantle and plumes: Constraints from
830 basalts, picrites, and komatiites. *Geochemistry Geophysics Geosystems* 8,
831 DOI:10.1029/2006GC001390.

832 Jacques, G., Hoernle, K., Gill, J., Hauff, F., Wehrmann, H., Garbe-Schonberg, D., van der
833 Bogaard, P., Bindeman, I., Lara, L.E., 2013. Across-arc geochemical variations in the
834 Southern Volcanic Zone, Chile (34.5 – 38.0 degrees S): Constraints on mantle wedge and
835 slab input compositions. *Geochimica et Cosmochimica Acta* 123, 218–243.

836 Jambon, A. 1994. Earth degassing and large-scale geochemical cycling of volatile elements. In:
837 Carroll, M.R., Holloway, J.R. (Eds.) *Volatiles in Magmas*, Rev. Mineral. 30, Mineral. Soc.
838 Am., Washington DC, pp 479–517.

839 Kamenetsky, V.S., Crawford, A.J., Meffre, S. (2001). Factors controlling chemistry of magmatic
840 spinel: An empirical study of associated olivine, Cr-spinel and melt inclusions from
841 primitive rocks. *Journal of Petrology* 42, 655–671.

842 Kamenetsky, V.S., Gurenko, A.A., Kerr, A.C., 2010. Composition and temperature of komatiite
843 melts from Gorgona Island constrained from olivine-hosted melt inclusions. *Geology* 38,
844 1003–1006.

845 Kent, A.J.R., Hauri, E., Woodhead, J., Hergt, J.M., 2009. Volatile contents of Belingewe
846 komatiites: Mantle volatile contents and the effects of degassing, *Geochimica et*
847 *Cosmochimica Acta* 73, A640.

848 Kerr, A.C., 2005. La Isla de Gorgona, Colombia: A petrological enigma? *Lithos* 84, 77–101.

849 Kerr, A.C., Arndt, N.T., 2001. A note on the IUGS reclassification of the high-Mg and picritic
850 volcanic rocks. *Journal of Petrology* 42, 2169–2171.

851 Kerr, A.C., Marriner, G.F., Arndt, N.T., Tarney, J., Nivia, A., Saunders, A.D., Duncan, R.A.,
852 1996. The petrogenesis of Gorgona komatiites, picrites and basalts: new field, petrographic
853 and geochemical constraints. *Lithos* 37, 245–260.

854 Kyser, T.K., Nisbet, E.G., Cameron, W.E., Gansser, A., Dietrich, V.J., 1987. Stable isotope
855 geochemistry and alteration of Cretaceous komatiitic and associated rocks from Gorgona
856 island, Colombia. *Geochemical Journal* 21, 253–259.

857 Ludwig, K.R. 2008. User's manual for Isoplot 3.70: A geochronological toolkit for Microsoft
858 Excel. Berkeley Geochronology Center, Special Publication No 4, 77 pp.

859 Martin, E., Bindeman, I. Grove, T.L., 2011. The origin of high-Mg magmas in Mt. Shasta and
860 Medicine Lake volcanoes, Cascade Arc (California): higher and lower than mantle oxygen
861 isotope signatures attributed to current and past subduction. *Contributions to Mineralogy
862 and Petrology* 162, 945–960.

863 Mathez, E.A., 1976. Sulfur solubility and magmatic sulfides in submarine basalt glasses. *Journal
864 of Geophysical Research* 81, 4269–4276.

865 Mathey, D., Lowry, D., Macpherson, C., 1994. Oxygen isotope composition of mantle peridotite.
866 *Earth and Planetary Science Letters* 128, 231–241.

867 Matthews, A., Stolper, E.M., Eiler, J.M., Epstein, S., 1998. Oxygen isotope fractionation among
868 melts minerals and rocks. *Mineralogical Magazine* 62A, 971–972 (Goldschmidt Conference
869 Extended Abstract).

870 McDonough, W.F., Ireland T.R., 1993. Intraplate origin of komatiites inferred from trace
871 elements in glass inclusions. *Nature* 365, 432–434.

872 Mironov, N., Portnyagin, M., Botcharnikov, R., Gurenko, A., Hoernle, K., Holtz, F., 2015.
873 Quantification of the CO₂ budget and H₂O–CO₂ systematics in subduction-zone magmas
874 through the experimental hydration of melt inclusions in olivine at high H₂O pressure. *Earth
875 and Planetary Science Letters* 425, 1–11.

876 Moore, L.R., Gazel, E., Tuohy, R., Lloyd, A.S., Esposito, R., Steele-MacInnis, M., Hauri, E.H.,
877 Wallace, P.J., Plank, T., Bodnar, R.J., 2015. Bubbles matter: An assessment of the
878 contribution of vapor bubbles to melt inclusion volatile budgets. *American Mineralogist*
879 100, 806–823.

880 Muehlenbachs, K., 1986. Alteration of the oceanic crust and the ^{18}O history of seawater. In:
881 Valley, J.W., Taylor Jr., H.P., O'Neil, J.R. (Eds.) *Stable Isotopes in High Temperature*
882 *Geological Processes*. Rev. Mineral, 16, Mineral. Soc. Am., Washington DC, pp 425–444.

883 Muehlenbachs, K., Anderson, A.T., Sigvaldason, G.E., 1974. Low- ^{18}O basalt from Iceland.
884 *Geochimica et Cosmochimica Acta* 38, 577–588.

885 Newman, S., Lowenstern, J.B., 2002. VolatileCalc: a silicate melt-H₂O-CO₂ solution model
886 written in Visual Basic for Excel. *Computers and Geosciences* 28, 597–604.

887 Parman, S.W., Grove, T.L., 2004. Harzburgite melting with and without H₂O: Experimental data
888 and predictive modeling. *Journal of Geophysical Research* 109, B02201, doi:
889 02210.01029/02003JB002566.

890 Parman, S.W., Grove, T.L., 2005. Komatiites in the plume debate. In: Foulger, G.R., Natland,
891 J.H., Presnall, D.C., Anderson, D.L. (Eds.) *Plates, Plumes, and Paradigms*, GSA Special
892 Publication 388, 249–256.

893 Parman, S.W., Dann, J.C., Grove, T.L., de Wit, M.J., 1997. Emplacement conditions of
894 komatiite magmas from the 3.49 Ga Komati Formation, Barberton Greenstone Belt. South
895 Africa. *Earth and Planetary Science Letters* 150, 303–324.

896 Peacock, S.M., Hervig, R.L., 1999. Boron isotopic composition of subduction-zone metamorphic
897 rocks. *Chemical Geology* 160, 281–290.

898 Portnyagin, M., Almeev, R., Matveev, S., Holtz, F., 2008. Experimental evidence for rapid water
899 exchange between melt inclusions in olivine and host magma. *Earth and Planetary Science*
900 *Letters* 272, 541–552.

901 Putlitz, B., Matthews, A., Valley, J.W., 2000. Oxygen and hydrogen isotope study of high-
902 pressure metagabbros and metabasalts (Cyclades, Greece): Implications for the subduction
903 of oceanic crust. *Contributions to Mineralogy and Petrology* 138, 114–126.

904 Révillon, S., Arndt, N.T., Chauvel, C., Hallot, E., 2000. Geochemical study of ultramafic
905 volcanic and plutonic rocks from Gorgona Island, Colombia: The plumbing system of an
906 oceanic plateau. *Journal of Petrology* 41, 1127–1153.

907 Révillon, S., Chauvel, C., Arndt, N.T., Pik, R., Martineau, F., Fourcade, S., Marty, B., 2002.
908 Heterogeneity of the Caribbean plateau mantle source: Sr, O and He isotopic compositions

909 of olivine and clinopyroxene from Gorgona Island. *Earth and Planetary Science Letters*,
910 91–106.

911 Savov, I.P., Ryan, J.G., D'Antonio, M., Kelley, K., Mattie, P., 2005. Geochemistry of
912 serpentinized peridotites from the Mariana Forearc – Conical Seamount, ODP Leg 125:
913 Implications for the elemental recycling at subduction zones. *Geochemistry Geophysics*
914 *Geosystems* 6, Q04J15, doi:10.1029/2004GC000777.

915 Savov, I.P., Ryan, J.G., D'Antonio, M., Fryer, P., 2007. Shallow slab fluid release across and
916 along the Mariana arc-basin system: Insights from geochemistry of serpentinized peridotites
917 from the Mariana Forearc. *Journal of Geophysical Research* 112, B09205,
918 doi:10.1029/2006JB004749.

919 Serrano, L., Ferrari, L., Martínez, M.L., Petrone, C.M., Jaramillo, C., 2011. An integrative
920 geologic, geochronologic and geochemical study of Gorgona Island, Colombia: Implications
921 for the formation of the Caribbean Large Igneous Province. *Earth and Planetary Science*
922 *Letters* 309, 324–336.

923 Shimizu, K., Komiya, T., Hirose, K., Shimizu, N., Maruyama, S., 2001. Cr-spinel, an excellent
924 micro-container for retaining primitive melts – implications for a hydrous plume origin for
925 komatiites. *Earth and Planetary Science Letters* 189, 177–188.

926 Shimizu, K., Shimizu, N., Komiya, K., Suzuki, K., Maruyama, S., Tatsumi, Y., 2009. CO₂-rich
927 komatiitic melt inclusions in Cr-spinels within beach sand from Gorgona Island, Colombia.
928 *Earth and Planetary Science Letters* 288, 33–43.

929 Smith, H.J., Spivack, A.J., Staudigel, H., Hart, S.R., 1995. The boron isotope composition of
930 altered oceanic crust. *Chemical Geology* 126, 119–135.

931 Sobolev, A.V., Danyushevsky, L.V., 1994. Petrology and geochemistry of boninites from the
932 north termination of the Tonga Trench: constraints on the generation conditions of primary
933 high-Ca boninite magmas. *Journal of Petrology* 35, 1183–1213.

934 Sobolev, A.V., Hofmann, A.W., 1999. Incompatible behavior of sulfur in ultra-depleted MORB.
935 *Ophioliti* 24, 166.

936 Sobolev, A.V., Hofmann, A.W., Kuzmin, D.V., Yaxley, G.M., Arndt, N.T., Chung, S.-L.,
937 Danyushevsky, L.V., Elliott, T., Frey, F.A., Garcia, M.O., Gurenko, A.A., Kamenetsky,

938 V.S., Kerr, A.C., Krivolutsкая, N.A., Matvienkov, V.V., Nikogosian, I.K., Rocholl, A.,
939 Sigurdsson, I.A., Sushchevskaya, N.M., Teklay, M., 2007. The amount of recycled crust in
940 sources of mantle-derived melts. *Science* 316, 412–417.

941 Sobolev, A.V., Hofmann, A.W., Brüggmann, B., Batanova, V.G., Kuzmin, D.V., 2008. A
942 quantitative link between recycling and osmium isotopes. *Science* 321, 536.

943 Sobolev, A.V., Asafov, E.V., Gurenko, A.A., Arndt, N.T., Batanova, V.G., Portnyagin, M.V.,
944 Garbe-Schönberg, D., Krashennnikov, S.P., 2016. Komatiites reveal an Archean hydrous
945 deep-mantle reservoir. *Nature* 531, 628–632, doi 10.1038/nature17152.

946 Stakes, D.S., Taylor, H.P., 1992. The northern Samail ophiolite: an oxygen isotope, microprobe,
947 and field study. *Journal of Geophysical Research* 97, 7043–7080.

948 Steele-Macinnis, M., Esposito, R., Bodnar, R.J., 2011. Thermodynamic model for the effect of
949 post-entrapment crystallization on the H₂O–CO₂ systematics of vapor-saturated, silicate melt
950 Inclusions. *Journal of Petrology* 52, 2461–2482.

951 Viljoen M. J. and Viljoen R. P. (1969a) Evidence for the existence of a mobile extrusive
952 peridotitic magma from the Komati Formation of the Onverwacht Group, Upper Mantle
953 Project. *Special Publication – Geological Society of South Africa* 2, 87-112.

954 Viljoen M. J. and Viljoen R. P. (1969b) The geology and geochemistry of the Lower Ultramafic
955 Unit of the Onverwacht Group and a proposed new class of igneous rocks, Upper Mantle
956 Project. *Special Publication – Geological Society of South Africa* 2, 55-85.

957 Wallace, P., Carmichael, I.S.E., 1992. Sulfur in basaltic magmas. *Geochimica et Cosmochimica*
958 *Acta* 56, 1863–1874.

959 Wallace, P.J., Kamenetsky, V.S. Cervantes, P., 2015. Melt inclusion CO₂ contents, pressures of
960 olivine crystallization, and the problem of shrinkage bubbles. *American Mineralogist* 100,
961 787–794.

962 Wang, Z., Eiler, J.M., 2008. Insights into the origin of low- $\delta^{18}\text{O}$ basaltic magmas in Hawaii
963 revealed from in situ measurements of oxygen isotope compositions of olivines. *Earth and*
964 *Planetary Science Letters* 269, 376–386.

965 Widom, E., Farquhar, J., 2003. Oxygen isotope signatures in olivines from Sao Miguel (Azores)
966 basalts: implications for crustal and mantle processes. *Chemical Geology* 193, 237–255.

967 Woodhead, J.D., Greenwood, P., Harmon, R.S., Stoffers, P., 1993. Oxygen isotope evidence for
968 recycled crust in the source of EM-type ocean island basalts. *Nature* 362, 809–813.

969 Yamaoka, K., Ishikawa, T., Matsubaya, O., Ishiyama, D., Nagaishi, K., Hiroyasu, Y., Chiba, H.,
970 Kawahata, H., 2012. Boron and oxygen isotope systematics for a complete section of
971 oceanic crustal rocks in the Oman ophiolite. *Geochimica et Cosmochimica Acta* 84,
972 543–559.

973
974

975 **Figure captions**

976 **Fig. 1.** Simplified geological map of the Gorgona island (modified after [Echeverría, 1980](#); [Kerr et](#)
977 [al., 1996](#); [Révillon et al., 2000](#)). Sampling locations are marked by sample numbers referred to in
978 the text.

979
980 **Fig. 2.** Elemental and oxygen isotopic composition of olivine from Gorgona picrite and
981 komatiite samples. Panels (A) and (D) represent inter- and intra-sample variations of forsterite
982 contents and $\delta^{18}\text{O}_{\text{Ol}}$ values, respectively. Shown here *error bars* represent the largest $\pm 2\sigma$
983 analytical uncertainty attained during replicate measurements of the San Carlos olivine standard
984 by EPMA (± 0.2 mol.% Fo) and SIMS ($\pm 0.4\text{‰}$ of $\delta^{18}\text{O}$). Panels (B) and (C) are variation
985 diagrams of NiO (B) and $\delta^{18}\text{O}_{\text{Ol}}$ (C) vs. Fo in the central parts and near the grain boundaries; (E)
986 cumulative probability density curves of $\delta^{18}\text{O}_{\text{Ol}}$ in *Ol core* and *Ol rim* parts calculated using
987 *Isoplot 3.70* ([Ludwig, 2008](#)). The *Gorgona Ol literature data* set (panel B) shows Fo and NiO
988 concentrations of olivines from [Kamenetsky et al. \(2010\)](#), [Gurenko and Kamenetsky \(2011\)](#), as
989 well as authors' unpublished data. The *shaded band* (panels C, D, E) denotes the range of typical
990 upper mantle olivine (4.8–5.4‰; [Mattey et al. 1994](#)) and of olivine in equilibrium with N-
991 MORB magmas (assuming olivine-melt fractionation of -0.4‰ and the N-MORB range of
992 5.2–5.8‰, [Eiler, 2001](#)). Dashed, numbered curves in panel (C) represent the Azores (1) and
993 Hawaii (2) *contamination trends* after [Wang and Eiler \(2008\)](#) and [Genske et al. \(2013\)](#),
994 respectively.

995
996 **Fig. 3.** Concentrations of CO_2 and H_2O dissolved in the olivine-hosted melt inclusions from
997 Gorgona komatiites measured by SIMS before correction for the loss in the shrinkage bubble of
998 CO_2 and H_2O (A) and after the correction applied (B) (see text). Isobars of melt compositions in
999 equilibrium with CO_2 - H_2O fluid (*solid lines*) and isopleths of fluid composition (dashed lines

1000 with labels returning molecular fraction of H₂O in the fluid) were calculated using *VolatileCalc*
1001 solution model (Newman and Lowenstern, 2002). Both isopleths and isobars were calculated for a
1002 magma having 47 wt.% SiO₂ at 1360°C, corresponding to the averaged values of the studied
1003 melt inclusions (Kamenetsky et al., 2010). Error bars represent average $\pm 2\sigma$ analytical
1004 uncertainty attained within three analytical sessions, i.e., $\pm 14\%$ relative for CO₂ and $\pm 12\%$
1005 relative for H₂O, and they are smaller than the size of the symbol, if not shown. The data from
1006 Shimizu et al. (2009) are shown for comparison.

1007
1008 **Fig. 4.** Relationships between concentrations of S, H₂O, Cl and F with FeO, SiO₂, Ce and Y in
1009 melt inclusions. (a) FeO vs. S variations. The *MORB & OIB* field presents S concentrations in
1010 presumably undegassed MORB and Hawaiian submarine tholeiitic and alkali basaltic glasses
1011 after Mathez (1976), Clague et al. (1995), Dixon et al. (1997) and Wallace and Carmichael
1012 (1992). Dashed curve represents sulfur solubility in basaltic melts based on the sulfide-saturated
1013 experiments of Haughton et al. (1974). (b) Ce vs. S, (c) SiO₂ vs. H₂O, (d) Y vs. H₂O and (e) F vs.
1014 Cl variations. The observed relationships do not support shallow depth contamination of the
1015 Gorgona high-Mg magmas, and rather favour a deep mantle origin of high volatile
1016 concentrations in the olivine-hosted melt inclusions, in agreement with Kamenetsky et al. (2010),
1017 Gurenko and Kamenetsky (2011) and Sobolev et al. (2016). The positive SiO₂-H₂O correlation
1018 may also be interpreted as reflecting gradually increasing degree of source melting at hydrous
1019 conditions.

1020
1021 **Fig. 5.** Averaged, single-grain oxygen isotope compositions of the studied Gorgona olivines. (A)
1022 $\delta^{18}\text{O}_{\text{Ol}}$ vs. Fo variation diagram, (B) probability density distribution curves of $\delta^{18}\text{O}_{\text{Ol}}$ values for
1023 olivine from komatiites and picrite GOR94-32.

1024

1025 **Fig. 6.** Oxygen versus boron isotopic compositions of olivine hosted melt inclusions from
1026 Gorgona komatiites. Subdivision of the inclusions on to “low- $\delta^{11}\text{B}$ ” and “high- $\delta^{11}\text{B}$ ” groups and
1027 their respective boron isotopic compositions are from [Gurenko and Kamenetsky \(2011\)](#). To infer
1028 oxygen isotope composition of the included melts, we used experimental data of [Matthews et al.](#)
1029 [\(1998\)](#) for komatiite to calculate O isotope fractionation factor between olivine and melt for the
1030 temperature range of 1320–1380 °C. Two-component mixing lines between the depleted MORB-
1031 type mantle (*MANT*), recycled crust (*REC*), serpentinised peridotite (*SERP1* and *SERP2*) and
1032 hypothetical oceanic crust fluids released at different temperatures (*FL1*, *FL2* and *FL3*) are
1033 shown (for end-member compositions see **Table S2.3**, *Supporting online material*). *Shaded grey*
1034 *field* represents the composition of the mantle, with $\delta^{11}\text{B}$ of $-10 \pm 2\text{‰}$ ([Gurenko and](#)
1035 [Kamenetsky, 2011](#) and references therein) and $\delta^{18}\text{O}$ of $5.5 \pm 0.5\text{‰}$, assuming a calculated
1036 oxygen isotope fractionation of -0.2‰ between olivine and high-Mg melt and the olivine range
1037 of 4.8–5.8‰, as defined in **Fig. 2**.

1038

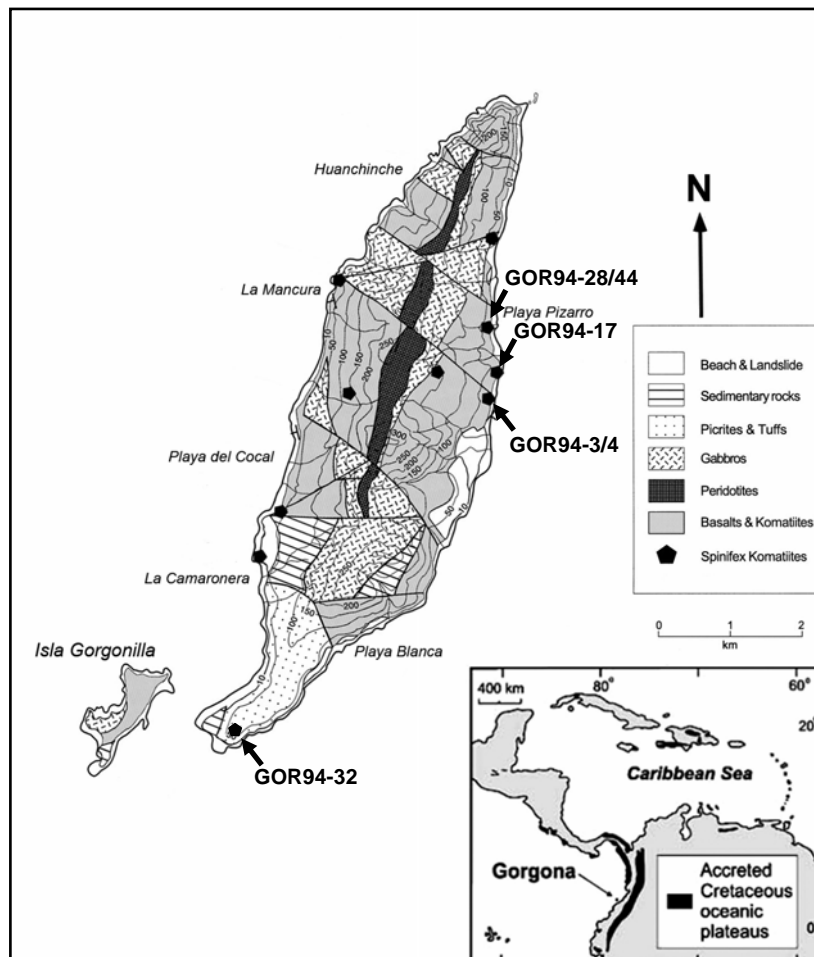


Fig. 1. Gurenko et al.

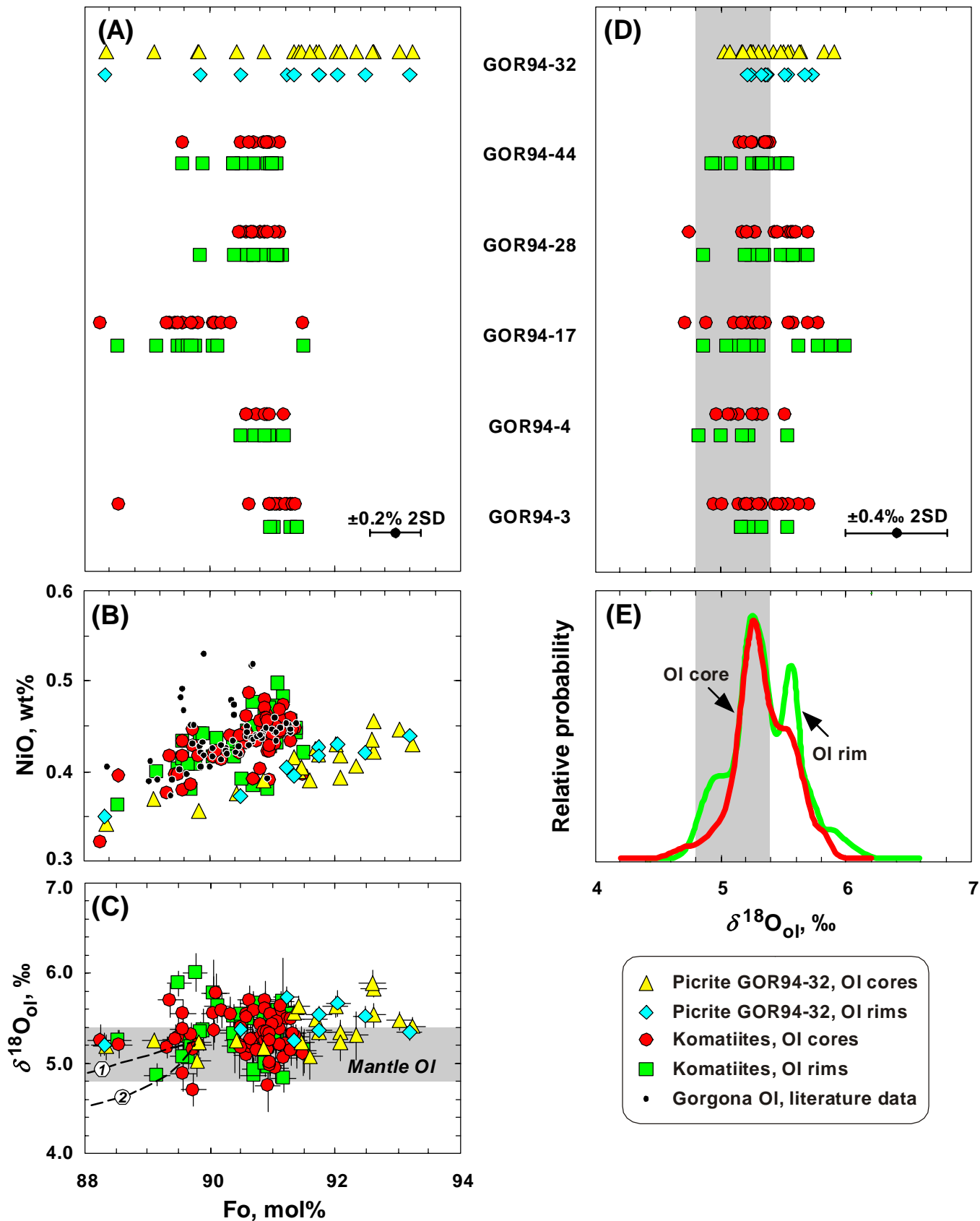


Fig. 2. Gurenko et al.

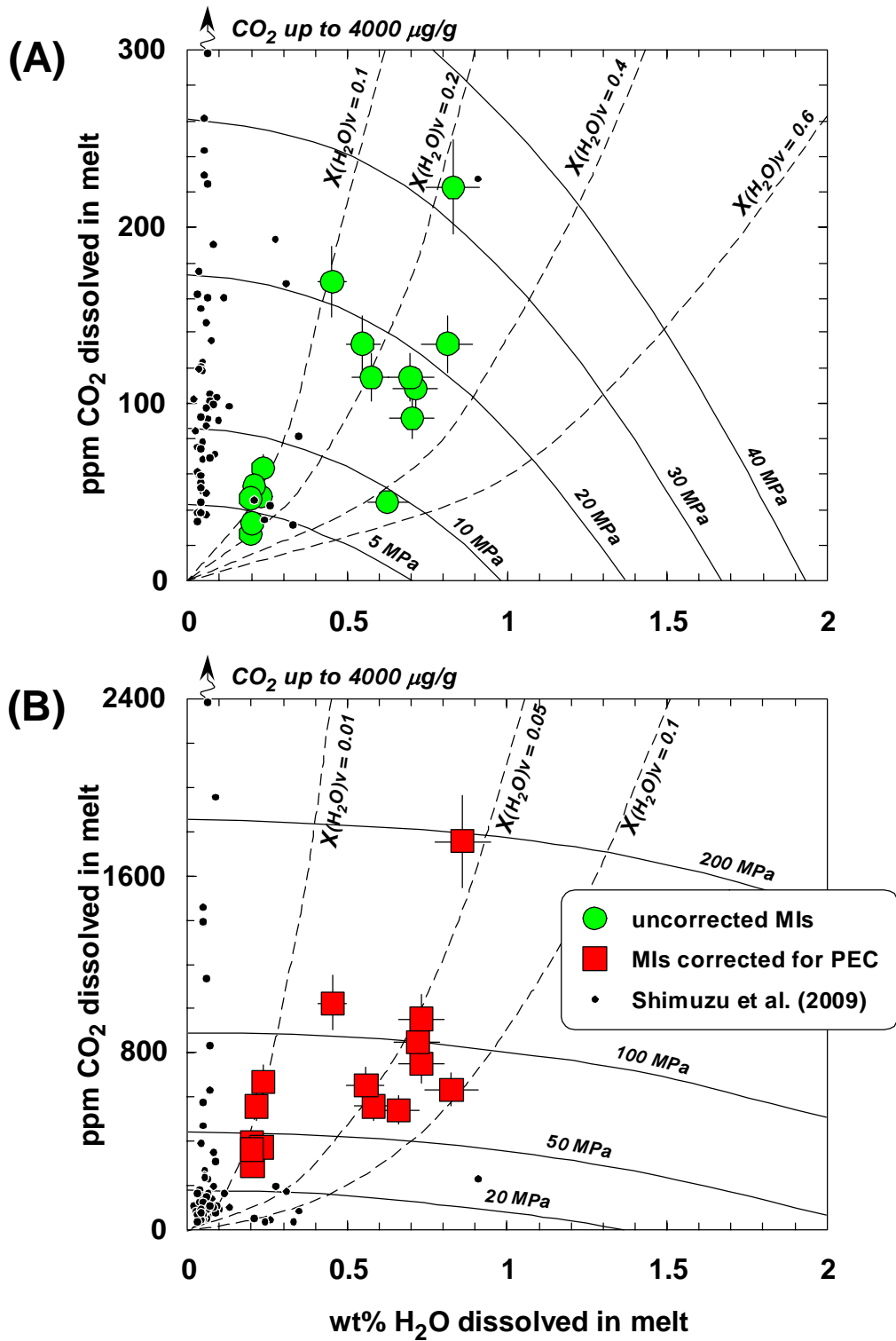


Fig. 3. Gurenko et al.

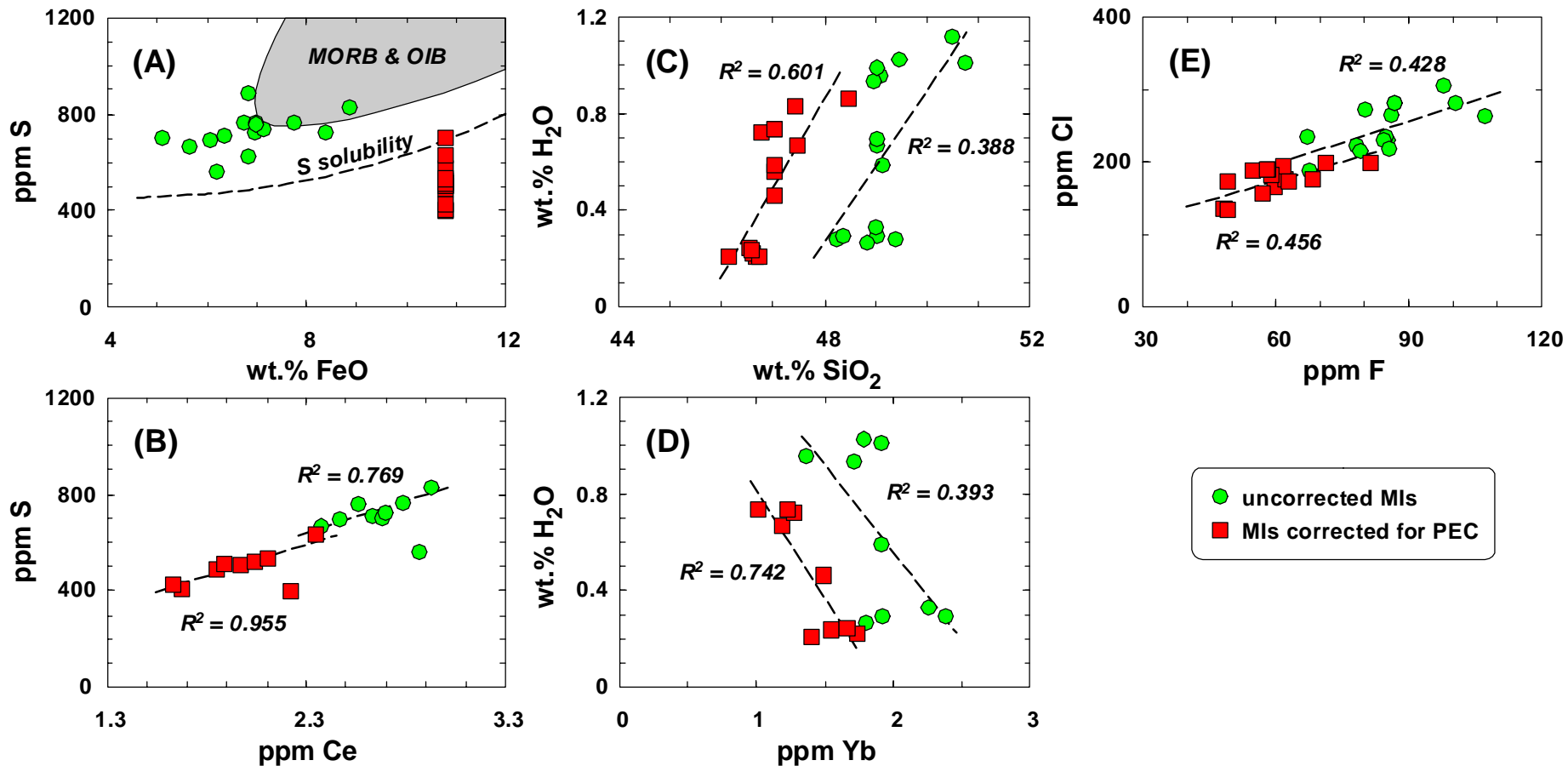


Fig. 4. Gurenko et al.

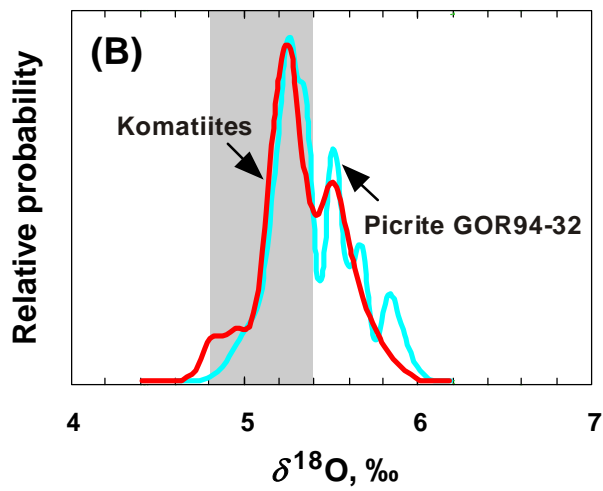
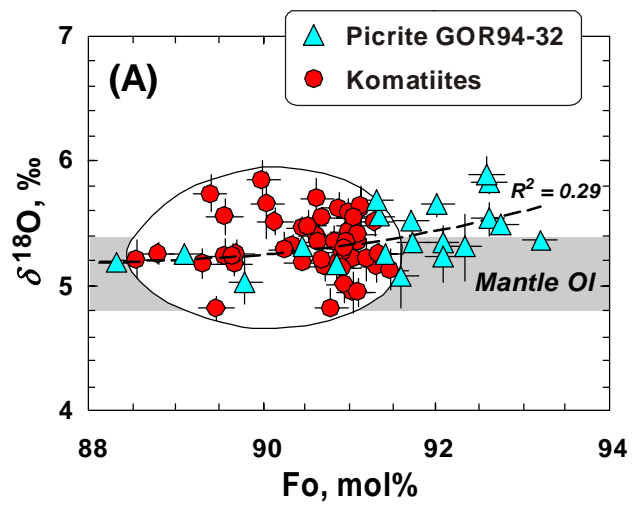


Fig. 5. Gurenko et al.

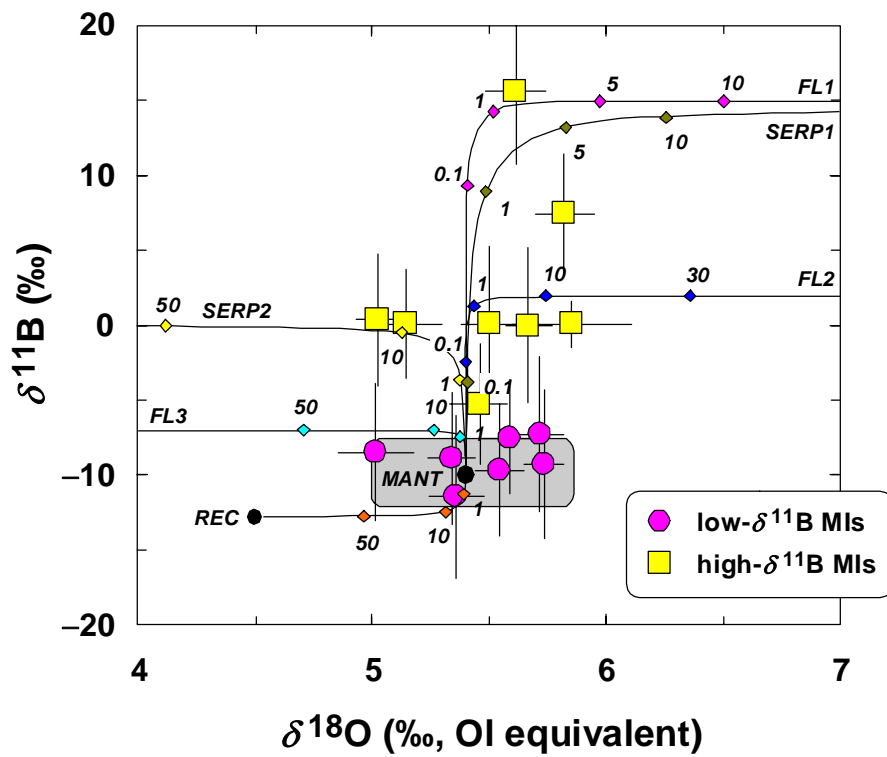


Fig. 6. Gurenko et al.

Supplementary material for online publication only

[Click here to download Supplementary material for online publication only: GOR d18O-OI SOM 4.1.pdf](#)